Causality Mapping Using Resting-state fMRI Reveals Hyperactivity and Hypoconnectivity in Schizophrenia Patients

Alishba Tahir[†], Wajiha Abdullah[1,†], Wjeeh ul Azeem[†], Muhammad Farhan Khalid[1], Turki Abualait[2], Sadia Shakil[3], Fayyaz Ahmed[4], Shahid Bashir[5,*], Safee Ullah Chaudhary[1,*]

[1] Biomedical Informatics and Engineering Research Laboratory, Department of Life Sciences, Syed Babar Ali School of Science and Engineering, Lahore University of Management Sciences, Lahore, Pakistan,

[2] College of Applied Medical Sciences, Imam Abdulrahman Bin Faisal University, Dammam, Saudi Arabia,

[3] Brno University of Technology, Brno, Czech Republic,

[4] Department of Statistics, University of Gujrat, Gujrat, Pakistan,

[5] Neuroscience Center, King Fahad Specialist Hospital Dammam, Dammam, Saudi Arabia.

[†] **Co-first authors**

*** Correspondence**:
Shahid Bashir
Neuroscience Center, King Fahad Specialist Hospital Dammam, Dammam, Saudi Arabia.
P.O. Box 15215, Dammam 31444, Saudi Arabia
ORCID No: https://orcid.org/0000-0001-6286-6895
E-mail: shahidbpk13@gmail.com
Tel.: +966 13 8442222 (Ext. 2423)

Safee Ullah Chaudhary
Biomedical Informatics Research Laboratory, Department of Biology, Syed Babar Ali School of Science and Engineering, Lahore University of Management Sciences, Lahore, Pakistan
ORCID No: https://orcid.org/0000-0002-3758-6581
Email: safee.ullah.chaudhary@gmail.com
Tel.: +92 321 4255171

Keywords: Schizophrenia, Frontal lobe, Basal ganglia, Ventricular system, Cerebellum, Granger causality, Vector auto regression, Resting-state functional magnetic resonance imaging, Functional connectivity.

Abstract

Schizophrenia (SZ) is a debilitating disorder in which patients exhibit psychotic behavior due to aberrant connectivity between different regions of the brain. Advances in neuroimaging have now enabled the diagnosis and analysis of SZ in order to elucidate the whole brain functional connectivity networks. In the present study, we have used resting-state functional magnetic resonance imaging (rs-fMRI) to elucidate the causal relationships amongst the differentially activated brain regions between SZ patients (n=10) and healthy controls (n=10). Vector auto-regression (VAR) model and Granger causality (GC) were then applied to construct a functional connectivity network and analyze the causal effects in SZ patients. Our results revealed that the average voxel activation in the frontal lobe (FL), basal ganglia (BG), and ventricular system (VS) was significantly higher in patients indicating hyper-activity as compared to controls. Conversely, cerebellum white matter (CBWM) showed higher activation in the controls as compared to patients. A higher Pearson correlation was observed between the controls as compared to patients while VAR and GC showed higher functional connectivity among all the regions of interest (ROIs) along with more causal relations in the controls. Finally, mediation analysis showed that right middle superior frontal gyrus acts as a strong partial mediator between left accumbens area and left middle superior frontal gyrus. Taken together, this study decodes the dysregulated brain activity in schizophrenia showing hyperactivation in patients when compared with the healthy controls which leads to alterations in neural connections resulting in hypoconnectivity.

1 Introduction

Schizophrenia (SZ) is a chronic mental disorder that affects over 24 million people across the globe (*Schizophrenia*, no date). The disease onset may begin during late adolescence and has a lifetime prevalence of 2.3% (*The epidemiology of early schizophrenia. Influence of age and gender on onset and early course - PubMed*, no date; Gogtay *et al.*, 2011; Subramaniam *et al.*, 2021). SZ-induced health deterioration is known to lower patients' life expectancy by 15-25 years besides degrading the overall quality of life (Wildgust, Hodgson and Beary, 2010; Vos *et al.*, 2017). SZ is divided into three types based on its clinical symptoms; 1. Positive symptoms including hallucinations, delusions, and disorganized behavior (*Psychiatry.org - DSM-5 Fact Sheets*, no date; Buckley and Miller, 2015; Bighelli *et al.*, 2018), 2. negative symptoms, such as flat affect and lack of movement etc. (Hare *et al.*, 2019), and 3. cognitive symptoms, such as disorganized thinking, confusion and memory loss (Hare *et al.*, 2019). Molecular investigations into the mechanistic underpinnings of SZ have led to discovery of several genetic alterations such as single-nucleotide polymorphisms and copy number variations in genes regulating dopaminergic neurotransmission in the brain (Li *et al.*, 2011; Warburton *et al.*, 2016).These molecular changes in SZ result in significant functional alterations in the neuronal connections between various regions of the brain and cause functional dysregulation (Konradi and Heckers, 2003; Lodge and Grace, 2011a; Beveridge and Cairns, 2012). In particular, altered patterns of neural activation in the prefrontal cortices, including the anterior cingulate cortex (ACC), the supplementary motor area (SMA), the pre-SMA, the parietal cortex, and the subcortical basal ganglia nuclei (Huang *et al.*, 2018; Hua *et al.*, 2020; Zhang *et al.*, 2020) are known indicators of SZ.

Chronic SZ causes rewiring of the brain thus altering the connections between different regions. Bioimaging research into SZ has reported a significant reduction in the functional connectivity (FC) amongst various regions of the brain(Koenig *et al.*, 2001; Skudlarski *et al.*, 2010; Zhou *et al.*, 2010;

Erdeniz *et al.*, 2017; Dong *et al.*, 2018). To decode the role of FC in SZ, researchers have studied the individual regions of the brain and evaluated their interrelationships towards uncovering the underpinning mechanisms. Individuals suffering from SZ are known to exhibit aberrations in regional connectivity which is caused by hyper/hypo activation in various regions of the brain [27–30]. The affected areas include all the major lobes of the brain including the frontal lobe (FL), temporal lobe (TL), occipital lobe and the memory center, the hippocampus (HC). FL which is known to be involved in cognition, memory, and higher order functions (Chayer and Freedman, 2001; Gillingham *et al.*, 2017), escalates the progression of SZ by lowering its activity (Corponi *et al.*, 2021) and impairing connectivity with the other regions of the brain (Jiang *et al.*, 2018). This results in induction of hallucinations and delusions which are two of the most prevalent symptoms observed in SZ patients (Jiang *et al.*, 2018). Shinba *et al.* and Chatterjee *et al.* investigated the abnormal functionality of FL in SZ and measured its activity through near-infrared spectroscopy (NIRS) (Shinba *et al.*, 2004) and fMRI (Chatterjee *et al.*, 2020), respectively. Such structural and functional dysfunction is not only limited to FL but also reported in other regions of the brain. For instance, OL which constitutes the visual cortex of the brain (Schneider *et al.*, 2019), has been reported to have reductions in the grey matter volume in the lateral and medial regions during SZ (Jiang *et al.*, 2018; Tordesillas-Gutierrez *et al.*, 2018). It is important to note that this atrophy manifests without any deterioration in the visual capacity of the patients (Johnson *et al.*, 2015). Similarly, TL is also affected during the progression of SZ; Spalthoff *et al.* reported altered gyrification in parts of TL including bilateral insula and temporal pole along with decreased grey matter volumes (Spalthoff, Gaser and Nenadić, 2018). HC, a part of the medial TL, is a key operating brain structure that is involved in memory retention and retrieval (Squire, Stark and Clark, 2004) (Huijgen and Samson, 2015) and its dysfunction furthers the cognitive symptoms related to SZ (Ghoshal and Conn, 2015). Note that HC plays a role in healthy and diseased brain as the dysfunction following SZ causes hippocampal dysregulation which leads to dopaminergic dysfunction (Lodge and Grace, 2007, 2011b; Grace, 2012).

Interestingly, in complete contrast with these findings, Salisbury *et al.* found higher resting state cerebral blood flow (rsCBF) in the bilateral temporal lobe and putamen indicating aberrant hyperactivity (Salisbury *et al.*, 2022). Zovetti *et al.* performed a task-based fMRI experiment and found out that patients' white matter tracts were hyperactivated inducing hyperconnectivity in areas encompassing the corpus callosum (Zovetti *et al.*, 2022). A meta-analysis by Wu *et al.* revealed multiple over-activated areas including bilateral dorsolateral prefrontal cortex, posterior parietal cortex, anterior cingulate cortex, anterior insula and supplementary motor area - areas making up the salience and central executive network (Wu and Jiang, 2020). Johnsen et al. tested brain activation in blood relatives of SZ patients through task-based fMRI in children and adolescents and found hyperactivation in the right dorsolateral prefrontal cortex and left caudate head, the left inferior frontal cortex, bilateral caudate, left inferior temporal gyrus, and bilateral frontal pole (Johnsen *et al.*, 2020). This hyperactivity was used to construct connectivity maps showing aberrant connectivity in SZ patients. Salvador et al., found over-connected regions with the default mode network (DMN) which exhibited the most hyperactivity. Other areas that have been also found to be over connected in brain disorders include several cortical and sub-cortical structures (Salvador *et al.*, 2010a). To exemplify, Koshiyama et al., reported over-connected brain networks between the major brain areas including the frontal, temporal and occipital lobe (Koshiyama *et al.*, 2020).

Researchers have also endeavored to assess white matter composition and identified aberrant activations in several key brain regions, particularly the frontal lobe (FL), which is involved in the facilitation of advanced cognitive processes (Brewer *et al.*, 2007). Brewer et al. conducted a longitudinal PET study and found an increased activation of the FL in SZ patients which could attribute towards the positive symptoms of SZ (Brewer *et al.*, 2007). Similarly, basal ganglia (BG) which are

present deep within the brain are also reported to be hypoactive and hyperactive as the disease progresses (Salvador *et al.*, 2010b). Changes in size and structure of BG have been reported in majority of the cases thus making it one of the key players in SZ. The ventricular system (VS), located near the BG, has shown larger volumes in SZ patients which can lead to a hyperactive state (Algunaid *et al.*, 2018). Another close by area is the cerebellum white matter (CWM) which is responsible for executive control and motor movement hence important from the point of view of psychopathology (Hariri, 2019). Cerebellum white matter (CWM) has been reported to increase in size contributing to the positive symptoms of SZ but with continued treatment it decreases over time (Christensen, Holcomb and Garver, 2004).

Till date, the distribution and variation in FC affecting neuronal communication and its underlying pathophysiological mechanisms, remains unclear (Rubinov and Bullmore, 2013). However, recent spatiotemporal investigations of the underlying neuropathological mechanisms of the diseased brain have provided some new insights (Minzenberg et al., no date; Snitz et al., 2005; Yoon et al., 2008; Lynall et al., 2010; Rubinov and Bullmore, 2013). In particular, studies leveraging technologies such as magnetic resonance imaging (MRI) (Sutcliffe et al., 2016; Vanes et al., 2019) and functional magnetic resonance imaging fMRI (del Re et al., 2019) have been employed to report a wide variety of abnormal structural and functional connections among anatomically distant regions of the brain in SZ patients (Sutcliffe et al., 2016; del Re et al., 2019; Vanes et al., 2019). Ralf et. al., employed a combination of fMRI and diffusion tensor imaging (DTI), and reported a modified structure-function relationship in SZ (Chayer and Freedman, 2001). Liang et al. further decoded the temporal associations between various regions of the brain and analyzed the FC by calculating multiple neuroimaging characteristics such as gray matter volume (Gillingham et al., 2017).

Towards investigating FC in SZ using rsfMRI, we have elucidated the causal relations between ROIs. For that, spatial independent component analysis (ICA) (Yang et al., 2020) was used to identify the significant features in fMRI followed by computing voxel activations for the whole brain. The results showed differential activations for 16 areas in patients which were used for further statistical analyses. A seed-based temporal correlation analysis (SCA) (Mannell et al., 2010) was used to assess time-series connections among the ROIs. Resting-state functional connectivity (rsFC) and causal interactions among the regions were evaluated through multivariate vector autoregression (VAR) (Granger, 1969) and Granger causality (GC)(Wismüller and Vosoughi, 2021). Our results from spatial ICA indicated a higher BOLD signal in FL, BG, VS and CWM in SZ patients. Pearson correlation showed more significant correlations in all ROIs in controls compared to the patients. Significantly increased functional connections in vector auto regression were also observed amongst the controls along with increased G-causal relations between ROIs. Lastly, mediation analysis revealed that right middle frontal superior gyrus acts as a partial mediator between left accumbens and left middle frontal gyrus in both patients and control cases with a stronger partial mediation in patients.

In conclusion, this study provides novel evidence of hyperactivity in all ROIs in SZ patients along with hypoconnectivity with decreased causal connections as the disease progresses. These causal inferences between the four selected regions of the brain expand our understanding of the resting-state FC (rsFC) in patients with SZ at the whole-brain level. This study also helps to characterize the FC among different regions of the brain and its variations in patients with SZ thereby providing valuable insights into the neural basis of SZ. Taken together, the study has the potential to direct SZ diagnosis through the identification of neuroimaging markers, decoding the functional connectivity networks and elucidating the causal interactions in the healthy as well as the diseased brain (Abboud, Noronha and Diwadkar, 2017), (Acar et al., 2019; Fan et al., 2021).

2 Methods

2.1 Participants

The study was approved by the local ethic committee of King Fahad Specialist Hospital Dammam (KFSHD) (NEU0334). A total of 20 male participants were selected (Age; 33.14 ± 9.96, mean ± SD), 10 of whom were healthy controls, and the others were schizophrenia (SZ) patients. Individuals from the healthy cohort were randomly chosen whereas the SZ patients were selected from home-grown psychiatric clinics and were clinically stable for two weeks prior to testing. The patients were previously diagnosed based on the DSM-IV (Bell, 1994) criteria followed by manual confirmation from an experienced research assistant. All participants gave written informed consent for participation. Participants were excluded if they: (a) met DSM-IV criteria for substance dependence or severe/moderate abuse during the prior six months; (b) had a clinically unstable or severe general medical disorder; or (c) had a history of head injury with documented neurological sequelae or loss of consciousness. Psychopathology was assessed by trained research assistants using the scale for the assessment of negative symptoms (SANS) and the scale for the assessment of positive symptoms (SAPS)(Andreasen *et al.*, 1995). Specific subscale scores were summed to derive measures of positive symptoms (hallucination and delusion subscales), disorganization (formal thought disorder, bizarre behavior, and attention subscales), and negative symptoms (flat affect, alogia, anhedonia and demotivation subscales).

2.2 Resting state functional magnetic resonance imaging

A Siemens Magnetom Verio 3T MRI clinical scanner (Siemens Healthineers) and a 12-channel phased-array head coil were used to acquire: (1) T1-weighted 3D magnetization-prepared rapid gradient-echo imaging (MPRAGE): Repetition Time (TR) = 1600 ms, Echo Time (TE) = 2.19 ms, inversion time = 900 ms, flip angle = 9°, acquisition plane = sagittal, voxel size = 1 × 1 × 1 mm^3, field of view (FOV) = 256 mm, acquired matrix = 256 × 256, acceleration factor (iPAT) = 2; (2) Fluid attenuated inversion recovery (FLAIR): TR = 9000 ms, TE = 128 ms, inversion time = 2500 ms, flip angle = 150°, acquisition plane = axial, slice thickness = 5mm, FOV = 220 mm, acquired matrix = 256 × 196, acceleration factor (iPAT) = 2. A total of 404 scans were taken per subject and the first four scans were discarded before performing the pre-processing which was carried out using statistical parametric mapping 12 (SPM 12).

To reduce the head movement in scans, each scan was corrected for motion against the mean image and realigned. Next, the scans were processed for spatial smoothing by taking the voxel averages. Gaussian kernel was used for images which had a normal distribution form. After spatial smoothing, the images were normalized according to the template image EPII (Echo-planar imaging) and specified to level one by using the binary condition and specified at level 2 by using all fifteen contrasts to undertake a group analysis.

2.3 Statistical Data Analysis

Mann Whitney test was used to compare the voxel activations between the controls and patients. To check for a correlation among the ROIs in both the groups, Pearson correlation was computed in MATLAB. To check if there were any time lagged causal connections amongst the ROIs vector auto-regression was computed and these results were further validated by Granger causality (GC). Spatial independent component analysis (ICA) was used to elucidate the connectivity patterns between all the brain areas in SPM towards determining their causal relationships (Gohel *et al.*, 2018). Seed based correlation analysis (SCA) was employed to evaluate the correlation between “seeds” (clusters of

neurons) that show concurrent activity in the 16 regions of interest (ROIs) that were differentially activated in patients compared to the controls(Beckmann *et al.*, 2005; Calhoun and Adali, 2012; Sheffield and Barch, 2016; Calhoun and de Lacy, 2017). Finally, vector auto-regression (VAR) and Granger causality (GC) were performed to study the bidirectional interaction amongst the ROIs and the time-lagged causal effects on each ROI, respectively(Zhou *et al.*, 2009; Guo, Liu, Liu, *et al.*, 2015; Silverstein, Bressler and Diwadkar, 2016).

2.4 Estimation of Granger Causality

GC(Seth, Barrett and Barnett, 2015) was modelled using equations 1 and 2 to analyze the fMRI data and elicit the causal connectivity between the activated regions of the brain. Specifically, in conventional regression models, any change in endogenous variable X_t results in a change in exogenous variable Y_t - that is, X_t causes Y_t and not vice versa (**Figure 1A**). To incorporate a bi-directional causality, vector auto-regression (VAR) models treat all variables equally such that X_t can cause Y_t (as well as their lags), and vice versa (**Figure 1B & C**). The VAR models for two of the four regions of interest (ROIs) i.e. FL and TL are defined in equations 1 and 2, respectively:

$$\mathrm{Y_t} = \beta_{10} - \beta_{12}\mathrm{X_t} + \gamma_{11}\mathrm{Y_{t-1}} + \gamma_{12}\mathrm{X_{t-1}} + \mu_{\mathrm{Yt}} \quad [1]$$

$$\mathrm{X_t} = \beta_{20} - \beta_{21}\mathrm{Y_t} + \gamma_{21}\mathrm{Y_{t-1}} + \gamma_{22}\mathrm{X_{t-1}} + \mu_{\mathrm{Xt}} \quad [2]$$

Where Y_t and X_t are stationary, μ_{Xt} and μ_{Yt} are not correlated and the resultant models are first order VAR models (Dimitrios Asteriou, no date).

Model [1] and [2] can be re-written as:

$$Y_t + \beta_{12}X_t = \beta_{10} + \gamma_{11}Y_{t-1} + \gamma_{12}X_{t-1} + \mu_{Yt} \quad [3]$$

$$\beta_{21}Y_t + X_t = \beta_{20} + \gamma_{21}Y_{t-1} + \gamma_{22}X_{t-1} + \mu_{Xt} \quad [4]$$

Or in the matrix form as (Arnold, Liu and Abe, 2007):

$$\begin{pmatrix} 1 & \beta_{12} \\ \beta_{21} & 1 \end{pmatrix}\begin{pmatrix} Y_t \\ X_t \end{pmatrix} = \begin{pmatrix} \beta_{10} \\ \beta_{20} \end{pmatrix} + \begin{pmatrix} \gamma_{11} & \gamma_{12} \\ \gamma_{21} & \gamma_{22} \end{pmatrix}\begin{pmatrix} Y_{t-1} \\ X_{t-1} \end{pmatrix} + \begin{pmatrix} \mu_{Yt} \\ \mu_{Xt} \end{pmatrix}$$

And in the short form as:

$$\beta Z_t = \gamma_0 + \gamma_1 Z_{t-1} + \mu_t \quad [5]$$

Pre-multiplication with β^{-1} gives:

$$Z_t = \beta^{-1}\gamma_0 + \beta^{-1}\gamma_1 Z_{t-1} + \beta^{-1}\mu_t \quad [6]$$

$$Z_t = A_0 + A_1 Z_{t-1} + \mu_t \quad [7]$$

Model [7], the reduced form of bivariate auto regression (BVAR) model, with all variables considered as stationary is written as $A = (\hat{A}_0, \hat{A}_1)^T$ by ordinary least squares (OLS) and the equation as:

$$\hat{A} = (Z_{t-1}\ Z_{t-1}^T)^{-1} Z_{t-1}\mathrm{Z_t} \quad [8]$$

Where $\hat{A} = \begin{pmatrix} \hat{A}_0 \\ \hat{A}_1 \end{pmatrix}$, and $\hat{\Sigma} = \frac{1}{n-k}\left(Z_t - \hat{A}Z_{t-1}\right)\left(Z_t - \hat{A}Z_{t-1}\right)^T$ and k = number of parameters.

Figure 1D and E show that Y_t may be affected by changes in lag values at X_{t-1}, X_{t-2} and X_{t-1}, Y_{t-1}, Y_{t-2} *and* Y_{t-1} and X_t may be effected by changes in lag values at X_{t-1}, X_{t-2}, X_{t-i}, Y_{t-1}, Y_{t-2} and Y_{t-i}

These GC models provide the following equations(Seth, Barrett and Barnett, 2015):

$$Y_t = a_1 + \sum_{i=1}^{n} \beta_i X_{t-i} + \sum_{j=1}^{m} \gamma_1 Y_{t-j} + e_{1t} \qquad [9]$$

$$X_t = a_2 + \sum_{i=1}^{n} \theta_i X_{t-i} + \sum_{j=1}^{m} \delta_j Y_{t-j} + e_{2t} \qquad [10]$$

The GC models estimated, using Python for equations [9] and [10], provided four possible parameters i.e.(i) the lagged X terms in equation [9] may be statistically different from zero as a group, (ii) the lagged Y terms in equation [10] may be statistically different from zero as a group, and the lagged Y terms in equation [1] may not be statistically different from zero, hence Y causes X, (iii) Both X and Y are statistically different from zero in [9] and [10], hence both X and Y cause each other. (iv) Both sets of X and Y terms are statistically not different from zero in [9] and [10], therefore both X and Y do not cause each other.

Following procedure was applied to equations [9] and [10] to calculate the G-causal relations amongst the ROIs:

Step 1: Regressing Y_t on lagged term Y_{t-j} as:

$$Y_t = a_1 + \sum_{j=1}^{n} \gamma_j Y_{t-j} + e_{1t} \qquad [11]$$

Step 2: Regressing Y_t on lagged terms of both, Y and X:

$$Y_t = a_2 + \sum_{j=1}^{n} \beta_i X_{t-i} + \sum_{j=1}^{m} \gamma_j Y_{t-j} + e_{2t} \qquad [12]$$

OLS models were used on equations [4] and [5] to calculate an unrestricted residual sum of square.

Step 3: Testing the effects on constant variables:

$$H_0: \sum_{j=1}^{n} \beta_i = 0 \quad (X_t = \text{FL does not cause } Y_t = \text{TL})$$

$$H_1: \sum_{i=1}^{n} \beta_i \neq 0 \quad (X_t = \text{FL causes } Y_t = \text{TL})$$

Step 4: calculating F-statistic:

$$F_c = \frac{(RSS_R - RSS_U) \,/\, m}{RSS_U/(n-k)}$$

where m = lags length at Y and k = number of parameters, and k = m + n + 1

Step 5: Applying Bayesian information criterion (BIC)

Lags length (m) was computed by the Bayesian Information Criterion (BIC) to compare models:

$$F_C > F_\alpha(m, n-k); \text{ Reject } H_0 \,,$$

BIC(m) criteria by using STATA.

This resulting novel GC model was applied to the results of the VAR model to establish the causal links between ROIs.

3 Results

3.1 Frontal lobe, basal ganglia, ventricular system and cerebellum white matter show hyperactivity in patients with Schizophrenia

To evaluate the differences between brain activation patterns in schizophrenic patients, resting state functional magnetic resonance imaging (rsfMRI) scans of 10 healthy controls (**Supplementary Data 1**) and 10 SZ patients (**Supplementary Data 2**) were obtained for 400 seconds. The recorded scans were pre-processed for realignment, spatial normalization, smoothing, and co-registration using statistical parametric mapping 12 (SPM12)(*SPM12 Software - Statistical Parametric Mapping*, no date). The voxel activations were deduced using the blood oxygen level dependent (BOLD) signal in the sixteen regions of interest (ROIs) which have been majorly anatomically categorized into frontal lobe (FL), basal ganglia (BG), ventricular system (VS), and cerebellum (CB). The voxel activations were then compared between healthy controls and SZ patients (**Figure 2**). Mann Whitney analysis showed significant differences in the average brain activity in the two groups for all ROIs. Right lateral ventricle, 3rd ventricle, left superior frontal gyrus and right superior frontal gyrus show the highest voxel activations in both groups, while right triangular part of the inferior frontal gyrus show the least activation in controls as well as the patients. Right cerebellum white matter is the only area that is more active in the controls as compared to the patients. Hence, patients exhibited an overall higher activity in all ROIs except one region, suggesting a hyperactive brain state.

3.2 Simultaneous activation patterns in ROIs differ significantly in Schizophrenia

To evaluate whether the aberrant activations observed within each ROI altered patterns of simultaneous activations, Pearson correlation was computed between ROIs for both controls and patients. In the VS, the right lateral ventricle (RLV) had the highest correlation with the right caudate ($r = 0.84384$, $p < 0.05$) of BG. In FL, the left posterior gyrus (LPG) showed the greatest correlation with the left accumbens area (LA) in BG. The inverse relationship was also the strongest amongst BG, as the left accumbens area (LA) had the strongest correlation with the left posterior orbital gyrus (LPOG) in the FL ($r = 0.90321$, $p < 0.05$). In the CWM, the strongest correlation was with the Right Superior Frontal Gyrus in the Frontal Lobe ($r = 0.68393$, $p < 0.05$). In the controls the right lateral ventricle sub region (RLVSR) of the VS exhibited the strongest correlation with the right caudate in the BG ($r = 0.85632$, $p < 0.05$). The FL had the strongest correlation with the right accumbens area (RA) of BG through the right superior frontal gyrus (RSFG) ($r = 0.74415$, $p < 0.05$). The right caudate in the BG had the greatest correlation with the right lateral ventricle (RLV) in VS ($r = 0.85632$, $p < 0.05$) and RCWM in the CWM had the greatest correlation with the right accumbens (RA) in the BG ($r = 0.65585$, $p < 0.05$). The results showed 222 significant correlations for SZ patients amongst all ROIs and 232 significant correlations in the controls thus indicating an altered ROI connectivity in SZ patients **(Figure 3)**.

3.3 Schizophrenia patients show hyper-connectivity between the ROIs

To examine the effect of altered correlation between ROIs, the temporal variations in functional connectivity (FC) between the ROIs were evaluated (Venkataraman *et al.*, 2012) at times *t*-1 and *t*-2 using vector auto-regression (VAR) model (Chen *et al.*, 2011), pair-wise, for all ROIs. Lags *t*-1 and *t*-2 were calculated through autocorrelation which showed connectivity with the other ROIs until *t*-2 seconds. In controls **(Figure 4A)**, FL exhibited strong causal connectivity between the right superior frontal gyrus (Right MSFG) and the right cerebellum white matter (Right CWM) ($t\text{-}2 = 0.236$, $p < 0.05$) whereas in the patients **(Figure 4B),** it was between the left superior frontal gyrus medial segment (left MSFG) and the Right CWM. For controls, BG had significant connectivity with the Right CWM ($t\text{-}1 = 0.1820448$, $p < 0.05$), whereas in patients' BG showed significant connectivity with the right lateral

ventricle in VS (t2 = 2103896, $p<0.05$). In controls, VS showed connectivity with the left accumbens (Left acc) in the BG (t-2= 0.1689018, $p < 0.05$) while in the patients, the 3rd ventricle had significant connectivity with the Right MSFG in the FL (t-1= 0.4509556, $p < 0.05$). Overall, controls had 41 significant connections between ROIs whereas patients had 38 indicating that functional connectivity is reduced in SZ. Hyperactivity in the patients did not accompany hyperconnectivity; the reduced connectivity led to hyperactivation in the ROI's. To validate the structural model of the brain connectivity network obtained through VAR and examine the intercausal effects of the ROIs in the controls and patients, Granger causality test was employed. In controls (**Figure 5A**) right lateral ventricle (RLV) G-caused right superior frontal gyrus (RSFG) (chi-square=35.337) in VS and G-caused right triangular inferior part of the frontal gyrus (RTriFG). RSFG G-caused third ventricle (chi-square=11.724) from the VS and RTriFG also G-caused right accumbens. Right caudate G-caused right frontal operculum (chi-square=20.462) in BG and right accumbens G-caused left opercular part of the inferior frontal gyrus (Left OpIFG). In patients (**Figure 5B**) RLV G-caused right accumbens (chi-square=20.748) in VS and right lateral ventricle also G-caused left OpIFG. RSFG G-caused right cerebellum white matter (chi-square=24.611) in FL and left superior frontal gyrus medial segment (LMSFG) G-caused right accumbens. Right caudate G-caused RSFG (chi-square=22.809) and right caudate also G-caused RTriFG. Overall, the controls had a total of 67 significant G-causal relationships compared to 52 in the patients confirming the results of the VAR model. The results of GC also indicate that loss in connections has a more magnified effect on the loss in useful causal connections as GC shows a more steep decrease in the causal interactions amongst the patients.

3.4 Right middle superior frontal gyrus acts as a partial mediator between left accumbens and left middle superior frontal gyrus

To investigate whether one of the ROIs mediates the relationship between the other ROIs, all possible combinations with 16 ROIs for mediation analyses were tested. Highest partial mediation was observed between nucleus accumbens (NA) (independent variable) and left middle superior frontal gyrus (LMSFG) (dependent variable) with right middle superior frontal gyrus (RMFSG) as a mediator for both controls and SZ patients (Figure 6A and B). However, in controls, RMSFG shows relatively lower mediation with the value of -0.0398 ($p<0.05$) whereas patients exhibited a stronger partial mediation value of 0.5704 ($p<0.05$) **(Figure 6)**. These results are indicative of an over-compensation in the patients as the regions of interest show a higher effect of removing one brain region in patients as compared to the controls. These results reconfirm that aberrant activation patterns lead to loss in functional connectivity.

4 Discussion

In this study, we aimed to establish the resting state functional connectivity (rsFC) patterns in healthy controls and schizophrenia (SZ) patients. Functional magnetic resonance imaging (fMRI) was used to detect the regional cerebral blood flow (rCBF) to calculate the average voxel activations for the controls as well as the patients. The data was then analyzed for computing the causal relations between ROIs using vector auto-regression (VAR) and Granger causality (GC).

Our results showed an increase in the voxel activations in the FL (frontal lobe), BG (basal ganglia), VS (ventricular system) and CB (cerebellum) in SZ patients suggesting hyperactivity in this patient cohort. Previously, both high and low voxel activations have been reported in SZ patients (Bobilev, Perez and Tamminga, 2020)(Holt *et al.*, 2006). Positron emission tomography (PET) scans show higher blood flow in the dentate gyrus (DG; a part of the HC) which receives sensory input from the brain to create memories (Pattabiraman *et al.*, 2021). The positive symptoms (hallucinations and delusions) of

SZ could also be a result of this altered activity. Frontal lobe (FL) is one of the areas that exhibits higher activation in SZ patients. The left posterior orbital gyrus (POG) exhibits hyper-activation in SZ patients and this contributes towards the symptoms of psychosis. While the literature does not specifically mention the left POG, there are several experiments that support hyperactivation in the FL(Brewer *et al.*, 2007). White matter disruptions have been reported as the main cause of functional abnormalities that arise with Schizophrenia (Cetin-Karayumak *et al.*, 2019). The basal ganglia (BG) have been consistently investigated as a potential contributor to the development of psychosis in schizophrenia. This region contains a significant population of dopamine neurons and is therefore a key target for the development of anti-psychotic drugs (Perez-Costas, Melendez-Ferro and Roberts, 2010). Aberrations in the basal ganglia have been observed in a variety of ways across schizophrenic patients. Notably, numerous studies have reported a reduction in both bilateral caudate size and volume in these individuals (Ellison-Wright *et al.*, 2008). In addition, altered white matter tract integration has been observed in the BG of schizophrenia patients when compared to healthy controls (Duan *et al.*, 2015). The bilateral caudate is an essential component of planning and task execution, a function that is significantly impaired in individuals with schizophrenia. Collectively, these alterations lead to aberrant activation patterns in the SZ patients.

Previous studies on SZ suggest that aberrant activation in the third ventricle and right lateral ventricle may be related to deficits in emotional regulation, executive function, and white matter integrity in schizophrenia (Minzenberg *et al.*, no date; Kubicki *et al.*, 2007a; Li *et al.*, 2007). Guo et al. reported reduced activation in the 3rd ventricle in SZ patients during emotional processing tasks indicating deficits in emotional regulation in SZ patients (Guo, Liu, Xiao, *et al.*, 2015). Mizenberg et al. found aberrant activation in the right lateral ventricle in individuals with SZ during tasks requiring executive function, which could be an indicator of suppressed cognitive processing in SZ patients (Minzenberg *et al.*, no date). DTI studies have also shown structural abnormalities in 3rd ventricle and right lateral ventricle, suggesting abnormalities in neural connectivity measured through fractional anisotropy (FA) in these regions (Kubicki *et al.*, 2007b). The strong association between the size of the third and lateral ventricles in individuals with schizophrenia implies that there may be a causal interaction between the two structures. The expansion of both the third and lateral ventricles may be more indicative of schizophrenia than the enlargement of either structure alone (Kubicki *et al.*, 2007b). Cerebellum has also shown to play a part in psychosis (Chang *et al.*, 2022) and studies have been done in order to ascertain the mechanism behind this dysfunction (Kim *et al.*, 2021). The reason why the activity for cerebellum is higher in patients than controls may be due to this dysfunction which misinterprets internal signal from auditory cortex as an external stimulus leading to hallucinations, a common symptom in schizophrenic patients (Bielawski and Bondurant, 2015).

The correlation matrices (**Figure 2)** show the voxel activation correlation amongst the ROIs and the results show an overall higher correlation for the controls. Previous research also supports these findings as patients with SZ have shown aberrant activation and altered connectivity between the ROIs (Duan *et al.*, 2015b; Jiang *et al.*, 2018; Zhao *et al.*, 2018; Kraguljac *et al.*, 2019; Bobilev, Perez and Tamminga, 2020) . This indicates that SZ increases the activation in all brain regions aberrantly leading to a lower correlation among them. It also supplements our findings of higher average voxel activations (**Figure 1**) in all ROIs.

In order to study the functional connectivity between the four ROIs in a time series, the study utilized vector auto-regression (VAR) model (**Figure 3**). VAR model shows hypo-connectivity in the patients supplementing previous research which also observed reduced degree centrality (DC) in patients with SZ compared to the controls. DC is an index used to identify the regions of the brain (at the whole-brain level) and display functional deficits in patients with SZ (Duan *et al.*, 2017) leading to reduced

414 functional connectivity. A lack of causal connectivity between the sensorimotor cortex (SMC) and
415 multiple regions of the default mode network (DMN) in patients with SZ was also observed (Wertz *et*
416 *al.*, 2019)(Kottaram *et al.*, 2019). Alterations to thalamic nuclei functional connectivity have also been
417 reported in the cortico-cerebellar-thalamo-cortical circuit pathways of patients(Woodward,
418 Karbasforoushan and Heckers, 2012) with SZ. GC was used to verify the above-mentioned results and
419 elucidate the causal effects of the ROIs and the results confirmed lowered connectivity amongst the
420 patients compared to the healthy controls. Previous research also supports our hypothesis stating that
421 functional connectivity and causal relations decrease through the prognosis of SZ (Wismüller and
422 Vosoughi, 2021). A study employing GC to identify and analyze the causal relations within the brain
423 reported a decrease in the functional connectivity between the targeted areas of the brain (Koshiyama
424 *et al.*, 2021). Hence, GC can be used as a technique to create a causal map of the connections in healthy
425 and diseased brain (Wismüller and Vosoughi, 2021). Lastly mediation analysis revealed a stronger
426 partial mediation in the patients which could be attributed towards loss in connectivity. A similar
427 pattern of altered rsFC has been observed throughout the entire brain in patients with SZ (Zhou *et al.*,
428 2008)(Zhuo *et al.*, 2018).

429 Amongst the strengths of this study, is its use of a combination of three different FC analysis methods
430 to investigate functional disconnections between various regions of the brain. However, the study does
431 have some limitations, which should be considered when interpreting the results. Most significantly,
432 the sample size in the present study is small. Additional longitudinal follow-up studies with larger
433 samples are needed to elucidate the alterations in FC between regions of the brain in patients with SZ.
434 Furthermore, many studies have reported different results (Jiang *et al.*, 2017) in the connectivity of
435 various regions of the brain and more research needs to be done with subjects from several ethnicities
436 so the differences can be recorded, and a standard diagnostic procedure can be implemented.

437 Together, these previous findings demonstrate that patients with SZ exhibit altered FC and effective
438 connectivity (EC) among several brain regions.

5 Tables

Table 1- Average voxel activation values for the patients and controls.

Average voxel activation			
Lobe	**Brain area**	**Activation in Patients**	**Activation in Controls**
Frontal Lobe	Left middle frontal gyrus	164.1021159	147.712822
	Right middle frontal gyrus	201.8846313	190.551855
	Right superior frontal gyrus medial segment	197.4187883	187.135653
	Left superior frontal gyrus medial segment	189.5789453	178.038965
	Right superior frontal gyrus	140.2225369	152.597001
	Right frontal operculum	182.1029834	158.985179
	Right triangular part of the inferior frontal gyrus	181.3794161	156.842199
	Right opercular part of the inferior gyrus	146.5843352	130.320612
	Left opercular part of the inferior gyrus	180.0882418	169.985293
	Left posterior orbital gyrus	196.0969863	180.433215
Basal ganglia	Right caudate	194.3676695	179.890929
	Left accumbens area	167.2095361	158.63256
	Right accumbens area	177.7478272	162.647039
Ventricular system	Right lateral ventricle	170.582288	154.732335
	3rd ventricle	188.2889905	167.356182
Cerebellum	Right cerebellum white matter	165.826113	150.275748

Table 2- Correlation co-efficients for 16 regions of interest. 1. Left posterior orbital gyrus, 2. Right lateral ventricle, 3. 3rd ventricle, 4. Right caudate, 5. Right cerebellum white matter, 6. Right accumbens area, 7. Left accumbens area, 8. Right triangular part of the inferior frontal gyrus, 9. Right superior frontal gyrus, 10. Left superior frontal gyrus medial segment, 11. Right superior frontal gyrus medial segment, 12. Right Frontal operculum, 13. Left middle frontal gyrus, 14. Right middle frontal gyrus, 15. Left opercular part of the inferior gyrus, 16. Right opercular part of the inferior gyrus**.** The upper half shows the controls, and the bottom half shows correlation values for the patients.

1	2	3	4	5	6	7	8	9	10	11	12	13	14	15	16
1.000	-0.599	-0.542	-0.245	0.495	0.742	0.378	0.839	0.862	0.808	0.822	0.336	0.851	0.851	0.856	0.721
-0.636	1.000	0.894	0.856	-0.060	-0.375	0.104	-0.624	-0.732	-0.320	-0.435	0.259	-0.633	-0.702	-0.663	-0.256
-0.380	0.750	1.000	0.743	-0.163	-0.389	0.108	-0.596	-0.718	-0.347	-0.465	0.186	-0.585	-0.682	-0.596	-0.244
-0.294	0.844	0.715	1.000	0.265	0.016	0.356	-0.260	-0.380	0.060	-0.058	0.510	-0.268	-0.333	-0.319	0.104
0.672	-0.486	-0.367	-0.297	1.000	0.656	0.401	0.544	0.518	0.624	0.599	0.476	0.466	0.528	0.440	0.579
0.852	-0.416	-0.185	-0.080	0.596	1.000	0.579	0.707	0.744	0.715	0.727	0.373	0.674	0.720	0.631	0.610
0.903	-0.574	-0.290	-0.263	0.665	0.915	1.000	0.299	0.307	0.489	0.413	0.433	0.400	0.315	0.327	0.404
0.795	-0.384	-0.202	-0.037	0.572	0.687	0.709	1.000	0.908	0.785	0.844	0.423	0.855	0.920	0.871	0.810
0.922	-0.685	-0.434	-0.313	0.684	0.799	0.864	0.813	1.000	0.800	0.867	0.303	0.912	0.974	0.874	0.705
0.898	-0.475	-0.209	-0.077	0.501	0.801	0.833	0.775	0.886	1.000	0.955	0.579	0.807	0.798	0.747	0.765
0.842	-0.365	-0.130	0.045	0.436	0.784	0.777	0.776	0.843	0.962	1.000	0.528	0.811	0.856	0.772	0.760

-0.358	0.777	0.644	0.776	-0.335	-0.253	-0.366	0.019	-0.356	-0.198	-0.093	1.000	0.358	0.366	0.307	0.700
0.898	-0.516	-0.261	-0.125	0.620	0.795	0.828	0.848	0.914	0.910	0.877	-0.184	1.000	0.935	0.915	0.740
0.862	-0.538	-0.310	-0.147	0.628	0.769	0.805	0.882	0.933	0.860	0.852	-0.154	0.948	1.000	0.896	0.763
0.819	-0.333	-0.142	-0.006	0.597	0.728	0.761	0.831	0.768	0.761	0.727	0.003	0.837	0.808	1.000	0.759
0.612	-0.114	0.040	0.206	0.383	0.576	0.559	0.840	0.629	0.651	0.676	0.318	0.729	0.776	0.802	1.000

Table 3(A)– Vector Autoregression (Average Controls). The table shows connectivity between 16 regions of interest. Right OpIFG: Right opercular part of the inferior gyrus, Right lat vent: Right lateral ventricle, Right CWM: Right cerebellum white matter, Left OpIFG: Left opercular part of the inferior gyrus, Right cau: Right caudate, Right TriFG: Right triangular part of the inferior frontal gyrus, 3rd vent: 3rd ventricle, Right MFG: Right middle frontal gyrus, Left acc: Left accumbens area, Left MSFG: Left superior frontal gyrus medial segment, Right MSFG: Right superior frontal gyrus medial segment, Left MFG: Left middle frontal gyrus, Right FO: Right frontal operculum, Left POrG: Left posterior orbital gyrus, Right acc: Right accumbens area, Right SFG: Right superior frontal gyrus, ROIs: Regions of interest, t: Time, Co-eff: Co-efficient, Std-error: Standard error, z: z-score

ROIs	t-1				t-2			
	Co-eff	Std-Error	z	p-value	Co-eff	Std-Error	z	p-value
1. Right OpIFG←Right cau	-.0433	.0871374	-0.50	0.619	.2054	.0880396	2.33	0.020
2. Right OpIFG←Right lat vent	-.1890	.0826249	-2.29	0.022	-.1887	.0832408	-2.27	0.023
3. Right OpIFG← 3rd vent	-.0171	.0303165	-0.56	0.572	.0902	.0306975	2.94	0.003
4. Left OpIFG←Right cau	.0743	.0921731	0.81	0.420	.1923	.0931274	2.07	0.039
5. Left OpIFG←Right lat vent	-.2386	.0873998	-2.73	0.006	-.2023	.0880513	-2.30	0.022
6. Left OpIFG←Right acc	.0231	.0538675	0.43	0.668	-.1447	.0533581	-2.71	0.007
7. Left OpIFG←3rd vent	-.0170	.0320685	-0.53	0.595	.0955	.0324716	2.94	0.003
8. Right MFG←Right cau	-.0277	.0850966	-0.33	0.744	.2312	.0859777	2.69	0.007
9. Right MFG←Right lat vent	-.2474	.0806897	-3.07	0.002	-.1618	.0812913	-1.99	0.046
10. Left MFG←Right cau	-.0965	.0979631	-0.99	0.324	.3452	.0989774	3.49	0.000
11. Left MFG←Right lat vent	-.2150	.09289	-2.31	0.021	-.2546	.0935825	-2.72	0.007
12. Left MFG←Right acc	.0211	.0572513	0.37	0.711	-.1319	.05671	-2.33	0.020
13. Left MFG←3rd vent	-.0154	.034083	-0.45	0.650	.0831	.0345113	2.41	0.016
14. Left MFG←Left acc	-.0166	.0536536	-0.31	0.756	.1172	.0528586	2.22	0.027
15. Right cau←Right CWM	.1820	.0713987	2.55	0.011	.1777	.0705207	2.52	0.012
16. Right cau←3rd vent	.0058	.0327924	0.18	0.859	.0823	.0332045	2.48	0.013
17. Right MSFG←Right cau	.0448	.1110214	0.40	0.686	.2307	.1121709	2.06	0.040

18. Right MSFG←Right MSFG	.4994	.132555	3.77	0.000	.2804	.1351265	2.08	0.038
19. Right MSFG←Right CWM	.1124	.0841007	1.34	0.181	.2364	.0830665	2.85	0.004
20. Right MSFG←3rd vent	-.0674	.0386262	-1.75	0.081	.0783	.0391116	2.00	0.045
21. Right MSFG←Left acc	-.0704	.0608056	-1.16	0.247	.1328	.0599045	2.22	0.027
22. Left MSFG←Right CWM	.1201	.0901566	1.33	0.183	.2006	.089048	2.25	0.024
23. Left MSFG←3rd vent	-.0737	.0414076	-1.78	0.075	.0946	.041928	2.26	0.024
24. Left MSFG←Left acc	-.0728	.0651841	-1.12	0.264	.1497	.0642181	2.33	0.020
25. Right lat vent←Right acc	.0345	.0553263	0.62	0.533	-.1265	.0548031	-2.31	0.021
26. Right lat vent←Right TriFG	.0116	.1023446	0.11	0.910	-.2309	.1027777	-2.25	0.025
27. Right lat vent←3rd vent	.00069	.032937	0.02	0.983	.0955	.0333509	2.86	0.004
28. Right lat vent←Left acc	-.0591	.0518496	-1.14	0.254	.1689	.0510812	3.31	0.001
29. Right SFG←Right lat vent	-.2580	.0928791	-2.78	0.005	-.2237	.0935715	-2.39	0.017
30. Right SFG←Left Acc	-.0363	.0536474	-0.68	0.498	.1319	.0528524	2.50	0.013
31. Right acc←Right CWM	.1603	.0941285	1.70	0.089	.1886	.0929711	2.03	0.042
32. Right TriFG←Right cau	-.0708	.0786123	-0.90	0.367	.1565	.0794262	1.97	0.049
33. Right TriFG←Right SFG	.0304	.0880628	0.35	0.730	-.1825	.0889938	-2.05	0.040

Table 3(B) – Vector Autoregression (Average Patients). The table shows connectivity between 16 regions of interest in the patients. Right OpIFG: Right opercular part of the inferior gyrus, Right lat vent: Right lateral ventricle, Right CWM: Right cerebellum white matter, Left OpIFG: Left opercular part of the inferior gyrus, Right cau: Right caudate, Right TriFG: Right triangular part of the inferior frontal gyrus, 3rd vent: 3rd ventricle, Right MFG: Right middle frontal gyrus, Left acc: Left accumbens area, Left MSFG: Left superior frontal gyrus medial segment, Right MSFG: Right superior frontal gyrus medial segment, Left MFG: Left middle frontal gyrus, Right FO: Right frontal operculum, Left POrG: Left posterior orbital gyrus, Right acc: Right accumbens area, Right SFG: Right superior frontal gyrus, ROIs: Regions of interest, t: Time, Co-eff: Co-efficient, Std-error: Standard error, z: z-score

ROIs	**t-1**				**t-2**			
	Co-eff	**Std-Error**	**z**	**p-valu**	**Co-eff**	**Std-Error**	**z**	**p-value**
1.Right OpIFG←Right CWM	.0557	.0300142	1.86	0.063	.0841172	.0306229	2.75	0.006
2.Right MFG←Right MFG	.5434	.1209978	4.49	0.000	.238683	.1212015	1.97	0.049
3.Left MFG←Right SFG	-.3748	.0848526	-4.42	0.000	.1731961	.0877795	1.97	0.048

4.Right cau←Right cau	.4165	.097813	4.26	0.000	.2204479	.0962971	2.29	0.022
5.Right MSFG←Right MSFG	.5197	.1555654	3.34	0.001	.4520271	.1545717	2.92	0.003
6.Right MSFG←Right FO	-.2769	.0981718	-2.82	0.005	.2084026	.0990462	2.10	0.035
7.Left MSFG←Right CWM	.2036	.0458128	4.44	0.000	.0946744	.0467419	2.03	0.043
8.Left MSFG←Right FO	-.2680	.1091011	-2.46	0.014	.2521826	.1100729	2.29	0.022
9.Right lat vent←Right lat vent	.0599	.0805626	0.74	0.456	.4517214	.0805998	5.60	0.000
10.Right SFG←Right SFG	.0511	.0888479	0.58	0.564	.2682422	.0919125	2.92	0.004
11.Right SFG←Left acc	.0239	.0575091	0.42	0.677	.1871581	.0583278	3.21	0.001
12.Right acc←Left OpIFG	-.0343	.09703	-0.35	0.724	-.2191728	.0949006	-2.31	0.021
13.Right acc←Right lat vent	-.4235	.0933591	-4.54	0.000	.2103896	.0934023	2.25	0.024
14.Right acc←Left acc	.02267	.0658204	0.34	0.730	.2531285	.0667575	3.79	0.000
15.Right TriFG←Right TriFG	.5040	.0953817	5.28	0.000	.2058574	.0944334	2.18	0.029
16.Right CWM←Right OpIFG	-.3703	.2052911	-1.80	0.071	.6117652	.2058626	2.97	0.003
17.Right CWM←Right FO	.5833	.144118	4.05	0.000	-.3674006	.1454016	-2.53	0.012
18.3rd vent←Right MSFG	-.0599	.2176579	-0.28	0.783	.4509556	.2162676	2.09	0.037
19.3rd vent←3rd vent	-.0298	.0612107	-0.49	0.626	.2104276	.0597504	3.52	0.000
20.3rd vent←Left acc	-.1434	.1051498	-1.36	0.172	.2434425	.1066468	2.28	0.022
21.Left acc←Left acc	.0615	.0779635	0.79	0.430	.4680959	.0790735	5.92	0.000
22.Left POrG←3rd vent	.0569	.0341825	1.66	0.096	-.0662206	.033367	-1.98	0.047
23.Left POrG←Left acc	-.0166	.0587198	-0.25	0.803	.1351963	.0595557	2.27	0.023
24.Left POrG←Left POrG	.3800	.0823871	4.61	0.000	.3183372	.085313	3.73	0.000
25.Right FO←Right CWM	.0572	.0358747	1.60	0.110	.1265024	.0366023	3.46	0.001
26.Right FO←Right FO	.3722	.0854341	4.36	0.000	.3410775	.086195	3.96	0.000

Table 4(A)- Granger Causality Test (Controls). The table shows intra-brain causal relations in the controls. Right OpIFG: Right opercular part of the inferior gyrus, Left OpIFG: Left opercular part of the inferior gyrus, Right MSFG: Right superior frontal gyrus medial segment, Right MFG: Right middle frontal gyrus, Left MSFG: Left superior frontal gyrus medial segment, Left POrG: Left posterior orbital gyrus, Left acc: Left accumbens area, Right Lat vent: Right lateral ventricle, Right SFG: Right superior frontal gyrus, Right acc: Right accumbens, Left MFG: Left middle frontal gyrus, Right cau: Right caudate, Right CWM: Right cerebellum white matter, Right TriFG: Right triangular part of the inferior frontal gyrus, 3rd vent: 3rd ventricle, Right FO: Right Frontal operculum, ALL: Causality

Equation	Excluded	Chi-square	Degree of Freedom	Probability > Chi-square
1.Right OpIFG	Left MSFG	6.0796	2	0.048
Right OpIFG	Right lat vent	27.403	2	0.000
Right OpIFG	Right cau	13.131	2	0.001

Right OpIFG	Right CWM	8.7141	2	0.013
Right OpIFG	Right FO	10.383	2	0.006
Right OpIFG	ALL	106.08	30	0.000
2.Left OpIFG	Right MFG	10.3	2	0.006
Left OpIFG	Left MSFG	8.8979	2	0.012
Left OpIFG	Right lat vent	33.467	2	0.000
Left OpIFG	Right acc	7.4683	2	0.024
Left OpIFG	Right CWM	8.7465	2	0.013
Left OpIFG	ALL	119.04	30	0.000
3.Right MSFG	Right MFG	8.537	2	0.014
Right MSFG	Left MSFG	8.6824	2	0.013
Right MSFG	Right lat vent	34.147	2	0.000
Right MSFG	Right cau	14.441	2	0.001
Right MSFG	Right FO	6.787	2	0.034
Right MSFG	ALL	141.58	30	0.000
4.Right MFG	Left OpIFG	9.2327	2	0.010
Right MFG	Left MSFG	12.995	2	0.002
Right MFG	Right lat vent	33.546	2	0.000
Right MFG	Left MFG	9.2983	2	0.010
Right MFG	Right cau	7.7397	2	0.021
Right MFG	ALL	143.18	30	0.000
5.Left MSFG	Right lat vent	16.772	2	0.000
Left MSFG	Right SFG	7.4045	2	0.025
Left MSFG	Right cau	18.413	2	0.000
Left MSFG	Right CWM	6.9891	2	0.030
Left MSFG	ALL	101.57	30	0.000
6.Left POrG	Right MFG	14.179	2	0.001
Left POrG	Left MSFG	7.0504	2	0.029
Left POrG	Right lat vent	28.421	2	0.000
Left POrG	Right cau	13.412	2	0.001
Left POrG	3rd vent	12.195	2	0.002
Left POrG	ALL	144.44	30	0.000
7.Left acc	Right MFG	9.1373	2	0.010
Left acc	Left MSFG	6.4232	2	0.040
Left acc	Right lat vent	24.126	2	0.000
Left acc	Right cau	9.5317	2	0.009
Left acc	Right CWM	6.5232	2	0.038
Left acc	3rd vent	13.918	2	0.001
Left acc	ALL	127.26	30	0.000
8.Right lat vent	Right OpIFG	8.8044	2	0.012
Right lat vent	Left MSFG	7.9549	2	0.019
Right lat vent	Right SFG	11.724	2	0.003
Right lat vent	Left MFG	9.0734	2	0.011
Right lat vent	Right cau	12.006	2	0.002
Right lat vent	Right CWM	8.9491	2	0.011
Right lat vent	Right TriFG	10.941	2	0.004
Right lat vent	ALL	143.69	30	0.000

9.Right SFG	Right MFG	8.7295	2	0.013
Right SFG	Right lat vent	35.337	2	0.000
Right SFG	Right cau	18.516	2	0.000
Right SFG	Right TriFG	6.3059	2	0.043
Right SFG	ALL	150.04	30	0.000
10.Right acc	Right lat vent	15.724	2	0.000
Right acc	Right cau	10.017	2	0.007
Right acc	Right TriFG	6.1234	2	0.047
Right acc	ALL	94.765	30	0.000
11.Left MFG	Right MFG	13.737	2	0.001
Left MFG	Right lat vent	17.277	2	0.000
Left MFG	Right cau	9.7921	2	0.007
Left MFG	Right CWM	13.893	2	0.001
Left MFG	ALL	142.76	30	0.000
12.Right cau	Left acc	10.132	2	0.006
Right cau	Right lat vent	10.179	2	0.006
Right cau	3rd vent	21.493	2	0.000
Right cau	ALL	87.256	30	0.000
13.Right CWM	Right SFG	7.3703	2	0.025
Right CWM	ALL	96.996	30	0.000
14.Right TriFG	Right lat vent	6.4619	2	0.040
15.3rd vent	Right OpIFG	7.5609	2	0.023
3rd vent	Right lat vent	37.733	2	0.000
3rd vent	Right SFG	9.9634	2	0.007
3rd vent	Right FO	6.9998	2	0.030
3rd vent	ALL	129.07	30	0.000
16.Right FO	Right OpIFG	9.1856	2	0.010
Right FO	Right MFG	6.4042	2	0.041
Right FO	Right lat vent	7.0622	2	0.029
Right FO	Right cau	20.462	2	0.000
Right FO	Right CWM	8.8226	2	0.012
Right FO	ALL	99.382	30	0.000

Table 4(B) – Granger Causality Test (Patients). The table shows intra-brain causal relations in the patients. Right OpIFG: Right opercular part of the inferior gyrus, Left OpIFG: Left opercular part of the inferior gyrus, Right MSFG: Right superior frontal gyrus medial segment, Right MFG: Right middle frontal gyrus, Left MSFG: Left superior frontal gyrus medial segment, Left POrG: Left posterior orbital gyrus, Left acc: Left accumbens area, Right Lat vent: Right lateral ventricle, Right SFG: Right superior frontal gyrus, Right acc: Right accumbens, Left MFG: Left middle frontal gyrus, Right cau: Right caudate, Right CWM: Right cerebellum white matter, Right TriFG: Right triangular part of the inferior frontal gyrus, 3rd vent: 3rd ventricle, Right FO: Right Frontal operculum, ALL: Causality

Equation	Excluded	Chi-square	Degree of Freedom	Probability > Chi-square

1.Right OpIFG	Right cau	13.123	2	0.001
Right OpIFG	ALL	77.53	30	0.000
2.Left OpIFG	Right lat vent	6.1263	2	0.047
Left OpIFG	ALL	76.164	30	0.000
3.Right MSFG	Right lat vent	6.1455	2	0.046
Right MSFG	Right SFG	13.451	2	0.001
Right MSFG	Right cau	20.511	2	0.000
Right MSFG	ALL	128.02	30	0.000
4.Right MFG	Right lat vent	6.4602	2	0.040
Right MFG	Right SFG	19.515	2	0.000
Right MFG	Right cau	15.408	2	0.000
Right MFG	3rd vent	9.8246	2	0.007
Right MFG	ALL	128.15	30	0.000
5.Left MSFG	Right lat vent	7.3486	2	0.025
Left MSFG	Right SFG	17.802	2	0.000
Left MSFG	Right cau	12.036	2	0.002
Left MSFG	ALL	71.077	30	0.000
6.Left POrG	Left acc	7.7016	2	0.021
Left POrG	Right lat vent	6.4294	2	0.040
Left POrG	Right SFG	11.613	2	0.003
Left POrG	Right cau	19.438	2	0.000
Left POrG	3rd vent	18.957	2	0.000
Left POrG	Right FO	8.3525	2	0.015
Left POrG	ALL	133.6	30	0.000
7.Left acc	Left POrG	7.6725	2	0.022
Left acc	Right SFG	13.988	2	0.001
Left acc	Right cau	27.731	2	0.000
Left acc	3rd vent	20.377	2	0.000
Left acc	Right FO	7.2638	2	0.026
Left acc	ALL	162.23	30	0.000
8.Right lat vent	Right SFG	15.211	2	0.000
Right lat vent	Right FO	10.039	2	0.007
Right lat vent	ALL	65.785	30	0.000
9.Right SFG	Right MSFG	6.3137	2	0.043
Right SFG	Left acc	8.8369	2	0.012
Right SFG	Right lat vent	7.5767	2	0.023
10.Right SFG	Right cau	22.809	2	0.000
Right SFG	Right TriFG	10.825	2	0.004
Right SFG	3rd vent	12.898	2	0.002
Right SFG	ALL	151.37	30	0.000
11.Right acc	Left OpIFG	8.5741	2	0.014
Right acc	Left MSFG	6.1715	2	0.046
Right acc	Right lat vent	20.748	2	0.000
Right acc	Right cau	6.2157	2	0.045
Right acc	Right TriFG	14.883	2	0.001
Right acc	ALL	108.39	30	0.000
12.Left MFG	ALL	83.196	30	0.000

13.Right cau	Right OpIFG	8.9789	2	0.011
Right cau	Right SFG	12.044	2	0.002
Right cau	Right TriFG	7.6104	2	0.022
Right cau	Right FO	16.49	2	0.000
Right cau	ALL	157.81	30	0.000
14.Right CWM	Right SFG	24.611	2	0.000
Right CWM	Right cau	11.155	2	0.004
Right CWM	Right TriFG	6.5353	2	0.038
Right CWM	Right FO	10.228	2	0.006
Right CWM	ALL	121.95	30	0.000
15.Right TriFG	Right lat vent	15.301	2	0.000
Right TriFG	Right cau	6.2818	2	0.043
Right TriFG	3rd vent	8.5096	2	0.014
Right TriFG	ALL	106.38	30	0.000
16.3rd vent	Right MFG	8.2841	2	0.016
3rd vent	Right lat vent	8.2368	2	0.016
3rd vent	Right CWM	6.4066	2	0.041
3rd vent	ALL	81.251	30	0.000
17.Right FO	Left acc	10.445	2	0.005
Right FO	Right cau	16.861	2	0.000
Right FO	ALL	70.743	30	0.000

Table 5- Mediation analysis for controls and patients. The table shows partial mediation in controls and patients. Left acc: Left accumbens area, Left MSFG: Left superior frontal gyrus medial segment, Right MSFG: Right superior frontal gyrus medial segment, Std-error: Standard error, * Significant.

	Type of Effect	Coefficient*	Std-Error	t-value	p-value	Mediation
Controls	**1.Direct effect (Left acc on Left MSFG)**	0.0691	0.0040	17.2897	0.0000	**Partial Mediation**
	2.Direct effect (Right MSFG on Left MSFG)	0.8975	0.0135	66.5977	0.0000	
	3.Direct effect (Left acc on Right MSFG)	-0.0743	0.0042	-17.507	0.0000	
	4.Indirect effect (Left acc on Left MSFG)	-0.0398	-	-	-	
Patients	**5.Direct effect (Left acc on Left MSFG)**	0.1974	0.0173	11.3788	0.0000	**Partial Mediation**
	6.Direct effect (Right MSFG on Left MSFG)	1.0227	0.0242	42.3007	0.0000	
	7.Direct effect (Left acc on Right MSFG)	-0.0567	0.0174	-3.2490	0.0013	
	8.Indirect effect (Left acc on Left MSFG)	0.5704	-	-	-	

6 References

Abboud, R., Noronha, C. and Diwadkar, V.A. (2017) 'Motor system dysfunction in the schizophrenia diathesis: Neural systems to neurotransmitters', *European Psychiatry*, 44, pp. 125–133. Available at: https://doi.org/10.1016/j.eurpsy.2017.04.004.

Acar, E. *et al.* (2019) 'Unraveling diagnostic biomarkers of schizophrenia through structure-revealing fusion of multi-modal neuroimaging data', *Frontiers in Neuroscience*, 13(MAY), p. 416. Available at: https://doi.org/10.3389/FNINS.2019.00416/BIBTEX.

Algunaid, R.F. *et al.* (2018) 'Schizophrenic patient identification using graph-theoretic features of resting-state fMRI data', *Biomedical Signal Processing and Control*, 43, pp. 289–299. Available at: https://doi.org/10.1016/j.bspc.2018.02.018.

Andreasen, N.C. *et al.* (1995) 'Correlational studies of the Scale for the Assessment of Negative Symptoms and the Scale for the Assessment of Positive Symptoms: an overview and update', *Psychopathology*, 28(1), pp. 7–17.

Arnold, A., Liu, Y. and Abe, N. (2007) 'Temporal causal modeling with graphical granger methods', *Proceedings of the ACM SIGKDD International Conference on Knowledge Discovery and Data Mining*, pp. 66–75. Available at: https://doi.org/10.1145/1281192.1281203.

Beckmann, C.F. *et al.* (2005) 'Investigations into resting-state connectivity using independent component analysis', *Philosophical Transactions of the Royal Society B: Biological Sciences*, 360(1457), pp. 1001–1013. Available at: https://doi.org/10.1098/RSTB.2005.1634.

Bell, C.C. (1994) 'DSM-IV: Diagnostic and Statistical Manual of Mental Disorders', *JAMA*, 272(10), pp. 828–829. Available at: https://doi.org/10.1001/jama.1994.03520100096046.

Beveridge, N.J. and Cairns, M.J. (2012) 'MicroRNA dysregulation in schizophrenia', *Neurobiology of disease*, 46(2), pp. 263–271. Available at: https://doi.org/10.1016/J.NBD.2011.12.029.

Bielawski, M. and Bondurant, H. (2015) 'Psychosis following a stroke to the cerebellum and midbrain: A case report', *Cerebellum and Ataxias*, 2(1), pp. 1–4. Available at: https://doi.org/10.1186/S40673-015-0037-8/FIGURES/1.

Bighelli, I. *et al.* (2018) 'Psychological interventions to reduce positive symptoms in schizophrenia: systematic review and network meta-analysis', *World psychiatry : official journal of the World Psychiatric Association (WPA)*, 17(3), pp. 316–329. Available at: https://doi.org/10.1002/WPS.20577.

Bobilev, A.M., Perez, J.M. and Tamminga, C.A. (2020) 'Molecular alterations in the medial temporal lobe in schizophrenia', *Schizophrenia Research*, 217, pp. 71–85. Available at: https://doi.org/10.1016/J.SCHRES.2019.06.001.

Brewer, W.J. *et al.* (2007) 'Increased prefrontal cerebral blood flow in first-episode schizophrenia following treatment: longitudinal positron emission tomography study', *The Australian and New Zealand journal of psychiatry*, 41(2), pp. 129–135. Available at: https://doi.org/10.1080/00048670601109899.

Buckley, P.F. and Miller, B.J. (2015) 'Schizophrenia Research: A Progress Report', *The Psychiatric*

clinics of North America, 38(3), pp. 373–377. Available at: https://doi.org/10.1016/J.PSC.2015.05.001.

Calhoun, V.D. and Adali, T. (2012) 'Multisubject independent component analysis of fMRI: A decade of intrinsic networks, default mode, and neurodiagnostic discovery', *IEEE Reviews in Biomedical Engineering*, 5, pp. 60–73. Available at: https://doi.org/10.1109/RBME.2012.2211076.

Calhoun, V.D. and de Lacy, N. (2017) 'Ten Key Observations on the Analysis of Resting-state Functional MR Imaging Data Using Independent Component Analysis', *Neuroimaging Clinics of North America*, 27(4), pp. 561–579. Available at: https://doi.org/10.1016/j.nic.2017.06.012.

Cetin-Karayumak, S. *et al.* (2019) 'White matter abnormalities across the lifespan of schizophrenia: a harmonized multi-site diffusion MRI study', *Molecular Psychiatry 2019 25:12*, 25(12), pp. 3208–3219. Available at: https://doi.org/10.1038/s41380-019-0509-y.

Chang, X. *et al.* (2022) 'Alterations of cerebellar white matter integrity and associations with cognitive impairments in schizophrenia', *Frontiers in Psychiatry*, 13. Available at: https://doi.org/10.3389/FPSYT.2022.993866/FULL.

Chatterjee, I. *et al.* (2020) 'Impact of ageing on the brain regions of the schizophrenia patients: an fMRI study using evolutionary approach', *Multimedia Tools and Applications*, 79(33–34), pp. 24757–24779. Available at: https://doi.org/10.1007/S11042-020-09183-Z/FIGURES/6.

Chayer, C. and Freedman, M. (2001) 'Frontal lobe functions', *Current Neurology and Neuroscience Reports 2001 1:6*, 1(6), pp. 547–552. Available at: https://doi.org/10.1007/S11910-001-0060-4.

Chen, G. *et al.* (2011) 'Vector autoregression, structural equation modeling, and their synthesis in neuroimaging data analysis', *Computers in Biology and Medicine*, 41(12), pp. 1142–1155. Available at: https://doi.org/10.1016/J.COMPBIOMED.2011.09.004.

Christensen, J., Holcomb, J. and Garver, D.L. (2004) 'State-related changes in cerebral white matter may underlie psychosis exacerbation', *Psychiatry Research: Neuroimaging*, 130(1), pp. 71–78. Available at: https://doi.org/10.1016/J.PSCYCHRESNS.2003.08.002.

Corponi, F. *et al.* (2021) 'Frontal lobes dysfunction across clinical clusters of acute schizophrenia', *Revista de Psiquiatría y Salud Mental* [Preprint]. Available at: https://doi.org/10.1016/J.RPSM.2021.12.002.

Dimitrios Asteriou, S.G.H. (no date) 'VAR Model', in *Applied econometrics*. 3rd edn. Red Globe Press, p. 552.

Dong, D. *et al.* (2018) 'Dysfunction of Large-Scale Brain Networks in Schizophrenia: A Meta-analysis of Resting-State Functional Connectivity', *Schizophrenia bulletin*, 44(1), pp. 168–181. Available at: https://doi.org/10.1093/SCHBUL/SBX034.

Duan, M. *et al.* (2015) 'Altered basal ganglia network integration in schizophrenia', *Frontiers in Human Neuroscience*, 9(OCT), p. 561. Available at: https://doi.org/10.3389/fnhum.2015.00561.

Duan, M. *et al.* (2017) '[Degree centrality of the functional network in schizophrenia patients]', *Sheng wu yi xue gong cheng xue za zhi = Journal of biomedical engineering = Shengwu yixue gongchengxue zazhi*, 34(6), pp. 837–841. Available at: https://doi.org/10.7507/1001-5515.201607062.

571 Ellison-Wright, I. *et al.* (2008) 'The anatomy of first-episode and chronic schizophrenia: An anatomical
572 likelihood estimation meta-analysis', *American Journal of Psychiatry*, 165(8), pp. 1015–1023.
573 Available at:
574 https://doi.org/10.1176/APPI.AJP.2008.07101562/ASSET/IMAGES/LARGE/T416T3.JPEG.

575 Erdeniz, B. *et al.* (2017) 'Decreased functional connectivity in schizophrenia: The relationship between
576 social functioning, social cognition and graph theoretical network measures', *Psychiatry Research:*
577 *Neuroimaging*, 270, pp. 22–31. Available at: https://doi.org/10.1016/J.PSCYCHRESNS.2017.09.011.

578 Fan, Y.S. *et al.* (2021) 'Individual-specific functional connectome biomarkers predict schizophrenia
579 positive symptoms during adolescent brain maturation', *Human Brain Mapping*, 42(5), pp. 1475–1484.
580 Available at: https://doi.org/10.1002/HBM.25307.

581 Ghoshal, A. and Conn, P.J. (2015) 'The hippocampo-prefrontal pathway: a possible therapeutic target
582 for negative and cognitive symptoms of schizophrenia', *http://dx.doi.org/10.2217/fnl.14.63*, 10(2), pp.
583 115–128. Available at: https://doi.org/10.2217/FNL.14.63.

584 Gillingham, S.M. *et al.* (2017) 'Assessing cognitive functioning in ALS: A focus on frontal lobe
585 processes', *Amyotrophic Lateral Sclerosis and Frontotemporal Degeneration*, 18(3–4), pp. 182–192.

586 Gogtay, N. *et al.* (2011) 'Age of Onset of Schizophrenia: Perspectives From Structural Neuroimaging
587 Studies', *Schizophrenia Bulletin*, 37(3), pp. 504–513. Available at:
588 https://doi.org/10.1093/SCHBUL/SBR030.

589 Gohel, S. *et al.* (2018) 'Frequency specific resting state functional abnormalities in psychosis', *Human*
590 *Brain Mapping*, 39(11), pp. 4509–4518. Available at: https://doi.org/10.1002/HBM.24302.

591 Grace, A.A. (2012) 'Dopamine system dysregulation by the hippocampus: Implications for the
592 pathophysiology and treatment of schizophrenia', *Neuropharmacology*, 62(3), pp. 1342–1348.
593 Available at: https://doi.org/10.1016/J.NEUROPHARM.2011.05.011.

594 Granger, C.W.J. (1969) 'Investigating Causal Relations by Econometric Models and Cross-spectral
595 Methods', *Econometrica*, 37(3), p. 424. Available at: https://doi.org/10.2307/1912791.

596 Guo, W., Liu, F., Liu, J., *et al.* (2015) 'Abnormal Causal Connectivity by Structural Deficits in First-
597 Episode, Drug-Naive Schizophrenia at Rest', *Schizophrenia Bulletin*, 41(1), pp. 57–65. Available at:
598 https://doi.org/10.1093/SCHBUL/SBU126.

599 Guo, W., Liu, F., Xiao, C., *et al.* (2015) 'Increased short-range and long-range functional connectivity
600 in first-episode, medication-naive schizophrenia at rest', *Schizophrenia Research*, 166(1–3), pp. 144–
601 150. Available at: https://doi.org/10.1016/J.SCHRES.2015.04.034.

602 Hare, S.M. *et al.* (2019) 'Salience-Default Mode Functional Network Connectivity Linked to Positive
603 and Negative Symptoms of Schizophrenia', *Schizophrenia bulletin*, 45(4), pp. 892–901. Available at:
604 https://doi.org/10.1093/SCHBUL/SBY112.

605 Hariri, A.R. (2019) 'The Emerging Importance of the Cerebellum in Broad Risk for Psychopathology',
606 *Neuron*, 102(1), pp. 17–20. Available at: https://doi.org/10.1016/J.NEURON.2019.02.031.

607 Holt, D.J. *et al.* (2006) 'Increased medial temporal lobe activation during the passive viewing of

608 emotional and neutral facial expressions in schizophrenia', *Schizophrenia Research*, 82(2–3), pp. 153–
609 162. Available at: https://doi.org/10.1016/J.SCHRES.2005.09.021.

610 Hua, M. *et al.* (2020) 'Disrupted pathways from limbic areas to thalamus in schizophrenia highlighted
611 by whole-brain resting-state effective connectivity analysis', *Progress in neuro-psychopharmacology*
612 *& biological psychiatry*, 99. Available at: https://doi.org/10.1016/J.PNPBP.2019.109837.

613 Huang, H. *et al.* (2018) 'Altered corticostriatal pathway in first-episode paranoid schizophrenia:
614 Resting-state functional and causal connectivity analyses', *Psychiatry Research: Neuroimaging*, 272,
615 pp. 38–45. Available at: https://doi.org/10.1016/J.PSCYCHRESNS.2017.08.003.

616 Huijgen, J. and Samson, S. (2015) 'The hippocampus: A central node in a large-scale brain network
617 for memory', *Revue Neurologique*, 171(3), pp. 204–216. Available at:
618 https://doi.org/10.1016/J.NEUROL.2015.01.557.

619 Jiang, Y. *et al.* (2017) 'Common and distinct dysfunctional patterns contribute to triple network model
620 in schizophrenia and depression: a preliminary study', *Progress in Neuro-Psychopharmacology and*
621 *Biological Psychiatry*, 79, pp. 302–310.

622 Jiang, Y. *et al.* (2018) 'Progressive reduction in gray matter in patients with schizophrenia assessed
623 with MR imaging by using causal network analysis', *Radiology*, 287(2), pp. 633–642. Available at:
624 https://doi.org/10.1148/RADIOL.2017171832/ASSET/IMAGES/LARGE/RADIOL.2017171832.FIG
625 4.JPEG.

626 Johnsen, L.K. *et al.* (2020) 'Alterations in Task-Related Brain Activation in Children, Adolescents and
627 Young Adults at Familial High-Risk for Schizophrenia or Bipolar Disorder - A Systematic Review',
628 *Frontiers in Psychiatry*, 11, p. 632. Available at:
629 https://doi.org/10.3389/FPSYT.2020.00632/BIBTEX.

630 Johnson, E.B. *et al.* (2015) 'The impact of occipital lobe cortical thickness on cognitive task
631 performance: An investigation in Huntington's Disease', *Neuropsychologia*, 79, pp. 138–146.

632 Kim, S.E. *et al.* (2021) 'Impaired cerebro-cerebellar white matter connectivity and its associations with
633 cognitive function in patients with schizophrenia', *npj Schizophrenia 2021 7:1*, 7(1), pp. 1–7. Available
634 at: https://doi.org/10.1038/s41537-021-00169-w.

635 Koenig, T. *et al.* (2001) 'Decreased functional connectivity of EEG theta-frequency activity in first-
636 episode, neuroleptic-naïve patients with schizophrenia: preliminary results', *Schizophrenia Research*,
637 50(1–2), pp. 55–60. Available at: https://doi.org/10.1016/S0920-9964(00)00154-7.

638 Konradi, C. and Heckers, S. (2003) 'Molecular aspects of glutamate dysregulation: implications for
639 schizophrenia and its treatment', *Pharmacology & therapeutics*, 97(2), p. 153. Available at:
640 https://doi.org/10.1016/S0163-7258(02)00328-5.

641 Koshiyama, D. *et al.* (2020) 'Neurophysiologic Characterization of Resting State Connectivity
642 Abnormalities in Schizophrenia Patients', *Frontiers in Psychiatry*, 11, p. 1350. Available at:
643 https://doi.org/10.3389/FPSYT.2020.608154/BIBTEX.

644 Koshiyama, D. *et al.* (2021) 'Neural network dynamics underlying gamma synchronization deficits in
645 schizophrenia', *Progress in Neuro-Psychopharmacology and Biological Psychiatry*, 107, p. 110224.

646 Available at: https://doi.org/10.1016/J.PNPBP.2020.110224.

647 Kottaram, A. *et al.* (2019) 'Brain network dynamics in schizophrenia: Reduced dynamism of the
648 default mode network', *Human Brain Mapping*, 40(7), pp. 2212–2228. Available at:
649 https://doi.org/10.1002/HBM.24519.

650 Kubicki, M. *et al.* (2007a) 'A review of diffusion tensor imaging studies in schizophrenia', *Journal of*
651 *psychiatric research*, 41(1–2), pp. 15–30. Available at:
652 https://doi.org/10.1016/J.JPSYCHIRES.2005.05.005.

653 Kubicki, M. *et al.* (2007b) 'A review of diffusion tensor imaging studies in schizophrenia', *Journal of*
654 *psychiatric research*, 41(1–2), pp. 15–30. Available at:
655 https://doi.org/10.1016/J.JPSYCHIRES.2005.05.005.

656 Li, M. *et al.* (2011) 'Genetic association and identification of a functional SNP at GSK3β for
657 schizophrenia susceptibility', *Schizophrenia research*, 133(1–3), pp. 165–171. Available at:
658 https://doi.org/10.1016/J.SCHRES.2011.09.013.

659 Li, X. *et al.* (2007) 'fMRI study of language activation in schizophrenia, schizoaffective disorder and
660 in individuals genetically at high risk', *Schizophrenia research*, 96(1–3), pp. 14–24. Available at:
661 https://doi.org/10.1016/J.SCHRES.2007.07.013.

662 Lodge, D.J. and Grace, A.A. (2007) 'Aberrant Hippocampal Activity Underlies the Dopamine
663 Dysregulation in an Animal Model of Schizophrenia', *The Journal of Neuroscience*, 27(42), pp. 11424
664 LP – 11430. Available at: https://doi.org/10.1523/JNEUROSCI.2847-07.2007.

665 Lodge, D.J. and Grace, A.A. (2011a) 'Hippocampal dysregulation of dopamine system function and
666 the pathophysiology of schizophrenia', *Trends in pharmacological sciences*, 32(9), pp. 507–513.
667 Available at: https://doi.org/10.1016/J.TIPS.2011.05.001.

668 Lodge, D.J. and Grace, A.A. (2011b) 'Hippocampal dysregulation of dopamine system function and
669 the pathophysiology of schizophrenia', *Trends in Pharmacological Sciences*, 32(9), pp. 507–513.
670 Available at: https://doi.org/10.1016/J.TIPS.2011.05.001.

671 Lynall, M.-E. *et al.* (2010) 'Functional connectivity and brain networks in schizophrenia', *Journal of*
672 *Neuroscience*, 30(28), pp. 9477–9487.

673 Mannell, M. V. *et al.* (2010) 'Resting state and task-induced deactivation: A methodological
674 comparison in patients with schizophrenia and healthy controls', *Human Brain Mapping*, 31(3), pp.
675 424–437. Available at: https://doi.org/10.1002/HBM.20876.

676 Minzenberg, M.J. *et al.* (no date) *Meta-analysis of 41 Functional Neuroimaging Studies of Executive*
677 *Function in Schizophrenia*, *jamanetwork.com*. Available at:
678 https://doi.org/10.1001/archgenpsychiatry.2009.91.

679 Pattabiraman, K. *et al.* (2021) 'Hippocampal Hyperactivity Emerges During a Critical Period in Mice',
680 *Biological Psychiatry*, 89(9), pp. S209–S210. Available at:
681 https://doi.org/10.1016/J.BIOPSYCH.2021.02.531.

682 Perez-Costas, E., Melendez-Ferro, M. and Roberts, R.C. (2010) 'Basal ganglia pathology in

683 schizophrenia: dopamine connections and anomalies', *Journal of Neurochemistry*, 113(2), pp. 287–
684 302. Available at: https://doi.org/10.1111/J.1471-4159.2010.06604.X.

685 *Psychiatry.org - DSM-5 Fact Sheets* (no date). Available at:
686 https://www.psychiatry.org/psychiatrists/practice/dsm/educational-resources/dsm-5-fact-sheets
687 (Accessed: 28 February 2023).

688 del Re, E.C. *et al.* (2019) 'Diffusion abnormalities in the corpus callosum in first episode
689 schizophrenia: Associated with enlarged lateral ventricles and symptomatology', *Psychiatry Research*,
690 277, pp. 45–51. Available at: https://doi.org/10.1016/J.PSYCHRES.2019.02.038.

691 Rubinov, M. and Bullmore, E. (2013) 'Schizophrenia and abnormal brain network hubs', *Dialogues in*
692 *Clinical Neuroscience*, 15(3), p. 339. Available at:
693 https://doi.org/10.31887/DCNS.2013.15.3/MRUBINOV.

694 Salisbury, D.F. *et al.* (2022) 'Pathological resting-state executive and language system perfusion in
695 first-episode psychosis', *NeuroImage: Clinical*, 36, p. 103261. Available at:
696 https://doi.org/10.1016/J.NICL.2022.103261.

697 Salvador, R. *et al.* (2010a) 'Overall brain connectivity maps show cortico-subcortical abnormalities in
698 schizophrenia', *Human Brain Mapping*, 31(12), pp. 2003–2014. Available at:
699 https://doi.org/10.1002/HBM.20993.

700 Salvador, R. *et al.* (2010b) 'Overall brain connectivity maps show cortico-subcortical abnormalities in
701 schizophrenia', *Human Brain Mapping*, 31(12), pp. 2003–2014. Available at:
702 https://doi.org/10.1002/HBM.20993.

703 *Schizophrenia* (no date). Available at: https://www.who.int/news-room/fact-
704 sheets/detail/schizophrenia (Accessed: 28 February 2023).

705 Schneider, C.L. *et al.* (2019) 'Survival of retinal ganglion cells after damage to the occipital lobe in
706 humans is activity dependent', *Proceedings of the Royal Society B*, 286(1897), p. 20182733.

707 Seth, A.K., Barrett, A.B. and Barnett, L. (2015) 'Granger causality analysis in neuroscience and
708 neuroimaging', *Journal of Neuroscience*, 35(8), pp. 3293–3297. Available at:
709 https://doi.org/10.1523/JNEUROSCI.4399-14.2015.

710 Sheffield, J.M. and Barch, D.M. (2016) 'Cognition and resting-state functional connectivity in
711 schizophrenia', *Neuroscience & Biobehavioral Reviews*, 61, pp. 108–120. Available at:
712 https://doi.org/10.1016/J.NEUBIOREV.2015.12.007.

713 Shinba, T. *et al.* (2004) 'Near-infrared spectroscopy analysis of frontal lobe dysfunction in
714 schizophrenia', *Biological Psychiatry*, 55(2), pp. 154–164. Available at:
715 https://doi.org/10.1016/S0006-3223(03)00547-X.

716 Silverstein, B.H., Bressler, S.L. and Diwadkar, V.A. (2016) 'Inferring the dysconnection syndrome in
717 schizophrenia: Interpretational considerations on methods for the network analyses of fMRI data',
718 *Frontiers in Psychiatry*, 7(AUG), p. 132. Available at:
719 https://doi.org/10.3389/FPSYT.2016.00132/BIBTEX.

720 Skudlarski, P. *et al.* (2010) 'Brain Connectivity Is Not Only Lower but Different in Schizophrenia: A
721 Combined Anatomical and Functional Approach', *Biological Psychiatry*, 68(1), pp. 61–69. Available
722 at: https://doi.org/10.1016/J.BIOPSYCH.2010.03.035.

723 Snitz, B.E. *et al.* (2005) 'Lateral and medial hypofrontality in first-episode schizophrenia: Functional
724 activity in a medication-naive state and effects of short-term atypical antipsychotic treatment',
725 *American Journal of Psychiatry*, 162(12), pp. 2322–2329. Available at:
726 https://doi.org/10.1176/appi.ajp.162.12.2322.

727 Spalthoff, R., Gaser, C. and Nenadić, I. (2018) 'Altered gyrification in schizophrenia and its relation
728 to other morphometric markers', *Schizophrenia research*, 202, pp. 195–202.

729 *SPM12 Software - Statistical Parametric Mapping* (no date). Available at:
730 https://www.fil.ion.ucl.ac.uk/spm/software/spm12/ (Accessed: 24 February 2023).

731 Squire, L.R., Stark, C.E.L. and Clark, R.E. (2004) 'The medial temporal lobe', *Annual review of*
732 *neuroscience*, 27, pp. 279–306. Available at:
733 https://doi.org/10.1146/ANNUREV.NEURO.27.070203.144130.

734 Subramaniam, M. *et al.* (2021) 'Lifetime Prevalence and Correlates of Schizophrenia and Other
735 Psychotic Disorders in Singapore', *Frontiers in psychiatry*, 12. Available at:
736 https://doi.org/10.3389/FPSYT.2021.650674.

737 Sutcliffe, G. *et al.* (2016) 'Neuroimaging Intermediate Phenotypes of Executive Control Dysfunction
738 in Schizophrenia', *Biological Psychiatry: Cognitive Neuroscience and Neuroimaging*, 1(3), pp. 218–
739 229. Available at: https://doi.org/10.1016/J.BPSC.2016.03.002.

740 *The epidemiology of early schizophrenia. Influence of age and gender on onset and early course -*
741 *PubMed* (no date). Available at: https://pubmed.ncbi.nlm.nih.gov/8037899/ (Accessed: 28 February
742 2023).

743 Tordesillas-Gutierrez, D. *et al.* (2018) 'The right occipital lobe and poor insight in first-episode
744 psychosis', *Plos One*, 13(6), p. e0197715.

745 Vanes, L.D. *et al.* (2019) 'Neural correlates of positive and negative symptoms through the illness
746 course: an fMRI study in early psychosis and chronic schizophrenia', *Scientific Reports 2019 9:1*, 9(1),
747 pp. 1–10. Available at: https://doi.org/10.1038/s41598-019-51023-0.

748 Venkataraman, A. *et al.* (2012) 'Whole brain resting state functional connectivity abnormalities in
749 schizophrenia', *Schizophrenia Research*, 139(1–3), pp. 7–12. Available at:
750 https://doi.org/10.1016/j.schres.2012.04.021.

751 Vos, T. *et al.* (2017) 'Global, regional, and national incidence, prevalence, and years lived with
752 disability for 328 diseases and injuries for 195 countries, 1990-2016: a systematic analysis for the
753 Global Burden of Disease Study 2016', *Lancet (London, England)*, 390(10100), pp. 1211–1259.
754 Available at: https://doi.org/10.1016/S0140-6736(17)32154-2.

755 Warburton, A. *et al.* (2016) 'A GWAS SNP for Schizophrenia Is Linked to the Internal MIR137
756 Promoter and Supports Differential Allele-Specific Expression', *Schizophrenia bulletin*, 42(4), pp.
757 1003–1008. Available at: https://doi.org/10.1093/SCHBUL/SBV144.

758 Wertz, C.J. *et al.* (2019) 'Disconnected and Hyperactive: A Replication of Sensorimotor Cortex
759 Abnormalities in Patients With Schizophrenia During Proactive Response Inhibition', *Schizophrenia*
760 *Bulletin*, 45(3), pp. 552–561. Available at: https://doi.org/10.1093/SCHBUL/SBY086.

761 Wildgust, H.J., Hodgson, R. and Beary, M. (2010) 'The paradox of premature mortality in
762 schizophrenia: new research questions.', *Journal of psychopharmacology (Oxford, England)*, 24(4
763 Suppl), pp. 9–15. Available at: https://doi.org/10.1177/1359786810382149.

764 Wismüller, A. and Vosoughi, M.A. (2021) 'Classification of schizophrenia from functional MRI using
765 large-scale extended Granger causality', p. 49. Available at: https://doi.org/10.1117/12.2582039.

766 Woodward, N.D., Karbasforoushan, H. and Heckers, S. (2012) 'Thalamocortical dysconnectivity in
767 schizophrenia', 169(10), pp. 1092–1099. Available at:
768 https://ajp.psychiatryonline.org/doi/abs/10.1176/appi.ajp.2012.12010056 (Accessed: 14 February
769 2022).

770 Wu, D. and Jiang, T. (2020) 'Schizophrenia-related abnormalities in the triple network: a meta-analysis
771 of working memory studies', *Brain Imaging and Behavior*, 14(4), pp. 971–980. Available at:
772 https://doi.org/10.1007/S11682-019-00071-1/FIGURES/1.

773 Yang, C. *et al.* (2020) 'Functional Alterations of White Matter in Chronic Never-Treated and Treated
774 Schizophrenia Patients', *Journal of Magnetic Resonance Imaging*, 52(3), pp. 752–763. Available at:
775 https://doi.org/10.1002/JMRI.27028.

776 Yoon, J.H. *et al.* (2008) 'Association of dorsolateral prefrontal cortex dysfunction with disrupted
777 coordinated brain activity in schizophrenia: Relationship with impaired cognition, behavioral
778 disorganization, and global function', *American Journal of Psychiatry*, 165(8), pp. 1006–1014.
779 Available at: https://doi.org/10.1176/appi.ajp.2008.07060945.

780 Zhang, M. *et al.* (2020) 'Abnormal amygdala subregional-sensorimotor connectivity correlates with
781 positive symptom in schizophrenia', *NeuroImage. Clinical*, 26. Available at:
782 https://doi.org/10.1016/J.NICL.2020.102218.

783 Zhou, B. *et al.* (2010) 'Brain functional connectivity of functional magnetic resonance imaging of
784 patients with early-onset schizophrenia', *Zhong nan da xue xue bao. Yi xue ban = Journal of Central*
785 *South University. Medical sciences*, 35(1), pp. 17–24. Available at:
786 https://doi.org/10.3969/J.ISSN.1672-7347.2010.01.003.

787 Zhou, Y. *et al.* (2008) 'Altered resting-state functional connectivity and anatomical connectivity of
788 hippocampus in schizophrenia', *Schizophrenia Research*, 100(1–3), pp. 120–132. Available at:
789 https://doi.org/10.1016/J.SCHRES.2007.11.039.

790 Zhou, Z. *et al.* (2009) 'Detecting directional influence in fMRI connectivity analysis using PCA based
791 Granger causality', *Brain Research*, 1289, pp. 22–29. Available at:
792 https://doi.org/10.1016/J.BRAINRES.2009.06.096.

793 Zhuo, C. *et al.* (2018) 'Altered resting-state functional connectivity of the cerebellum in
794 schizophrenia', *Brain Imaging and Behavior*, 12(2), pp. 383–389. Available at:
795 https://doi.org/10.1007/S11682-017-9704-0/FIGURES/3.

Zovetti, N. *et al.* (2022) 'Inefficient white matter activity in Schizophrenia evoked during intra and inter-hemispheric communication', *Translational Psychiatry*, 12(1), pp. 1–11. Available at: https://doi.org/10.1038/s41398-022-02200-9.

7 Declarations

Ethics approval and consent to participate.

IRB approval and number: The study was carried out in accordance with the code of international and local Ethics (Declaration of Helsinki). This study was reviewed and approved by the local ethics committee with approval no (NEU0334).

Patient consent for publication: The patient provided written informed consent for publication.

8 Abbreviations List

Right OpIFG: Right opercular part of the inferior gyrus
Right lat vent: Right lateral ventricle
Right CWM: Right cerebellum white matter
Left OpIFG: Left opercular part of the inferior gyrus
Right Cau: Right caudate
Right TriFG: Right triangular part of the inferior frontal gyrus
3rd vent: 3rd ventricle
Right MFG: Right middle frontal gyrus
Left acc: Left accumbens area
Left MSFG: Left superior frontal gyrus medial segment
Right MSFG: Right superior frontal gyrus medial segment
Left MFG: Left middle frontal gyrus
Right FO: Right frontal operculum
Left POrG: Left posterior orbital gyrus
Right acc: Right accumbens area
Right SFG: Right superior frontal gyrus
CWM: Cerebellum white matter
BG: Basal ganglia
VS: Ventricular system
FL: Frontal lobe
FC: Functional Connectivity

9 Conflict of Interest

None of the authors has any conflict of interest to disclose the data and the results.

10 Author Contributions

Study Design: Safee Ullah Chaudhary, Fayyaz Ahmad, Shahid Bashir, and Sadia Shakeel.

Data Processing: Wajiha Abdullah, Alishba Tahir, Wjeeh ul Azeem, Mirza Ibrahim Ahmad, Muhammad Farhan Khalid, and Fayyaz Ahmed.

Manuscript Writing: Wajiha Abdullah, Alishba Tahir, Wjeeh ul Azeem, Mirza Ibrahim Ahmad, Muhammad Farhan Khalid, Turki Abualait, Sadia Shakil, Shahid Bashir, Safee Ullah Chaudhary.

11 Funding

No funding was available to support this study.

12 Acknowledgments

The authors would like to thank participants and their family members for their time and their data.

13 Supplementary Material

Supplementary data 1 and 2 contain the fMRI results of controls and patients significantly.

14 Data Availability Statement

The datasets used and/or analyzed during the current study are available from the corresponding author on reasonable request.

15 Figure Captions

Figure 1 - Causal relations between variables. (A) Regression Model: X_t causes Y_t, (B) Vector Auto-regression Model: X_t can cause Y_t and vice versa, (C) Vector Auto-regression Model: X_t can cause Y_t and their lags, and vice versa, (D) Granger Causality Model-1: Y_t may be affected by changes in lag values at X_{t-1}, X_{t-2} and $X_{t-i...}$, and changes in lag values in Y_{t-1}, Y_{t-2} *and* Y_{t-j},.. where i and j represent different time points (E) Granger Causality Model-2: X_t may be affected by changes in lag values at Xt_{-1}, X_{t-2}, X_{t-i}… and changes in lag values in Y_{t-1}, Y_{t-2}, Y_{t-i}…

Figure 2 - Average Voxel Activation in Controls and Schizophrenia Patients. The bar graph shows average voxel activations in 16 ROIs for controls (grey) and patients (black).

Figure 3 - Correlation Between ROIs in Controls and Schizophrenia Patients. The heat map shows Person correlation between the ROIs in controls and SZ patients.

Figure 4 - Structural Connectivity in ROIs through vector autoregression model. Significant causality links between the ROIs in the patients (A) and the controls (B).

Figure 5 - Structural Connectivity in ROIs obtained through Granger Causality. Arrows show significant granger causality between ROIs for the controls (A) and patients (B).

Figure 6 - Mediation Analysis. **(A)** Mediation in controls between Left accumbens area, right MSFG, and left MSFG, **(B)** Mediation in patients between Left accumbens area, right MSFG, and left MSFG.

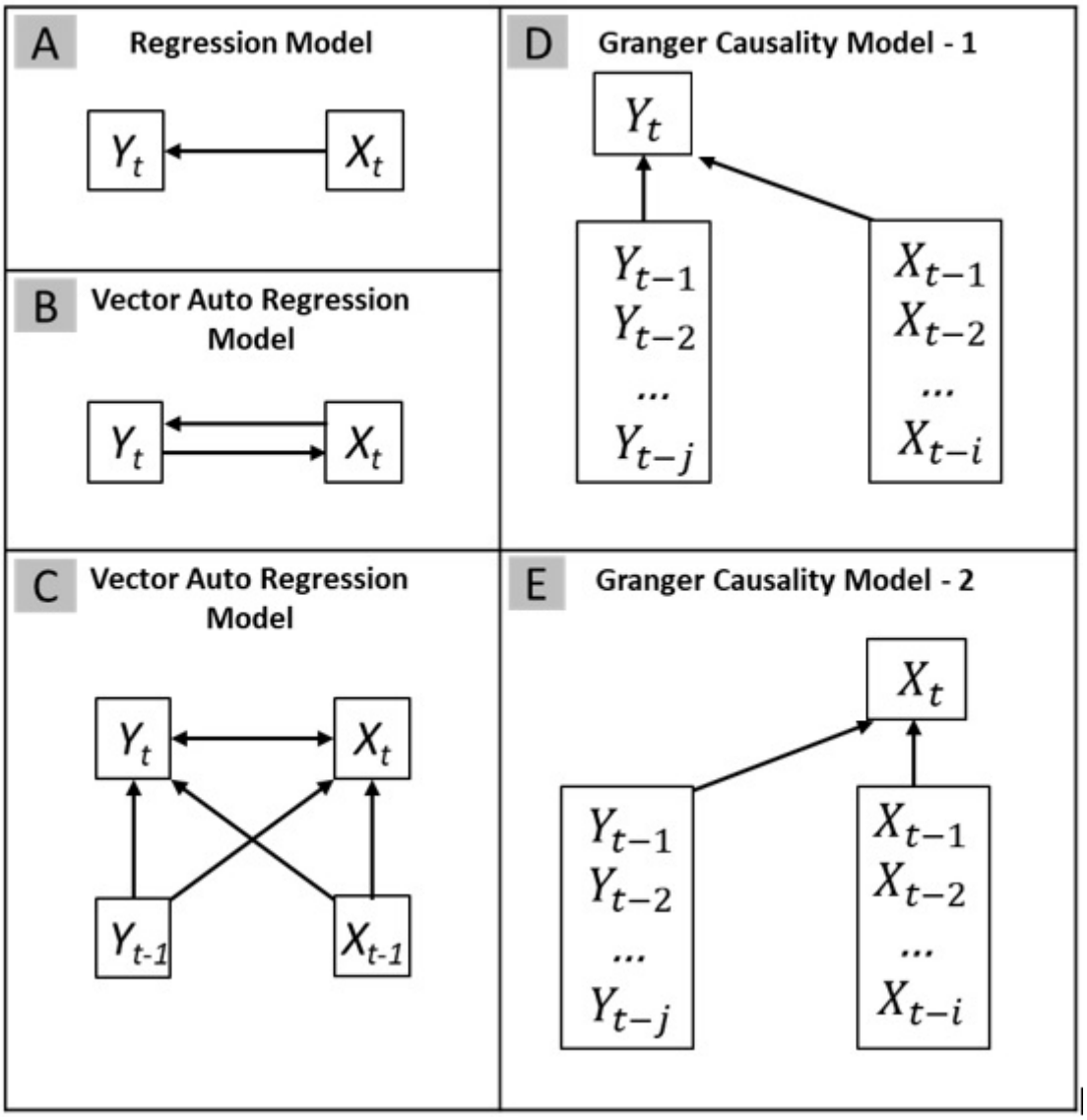

Figure 1 - Causal relations between variables. (A) Regression Model: X_t causes Y_t, (B) Vector Auto-regression Model: X_t can cause Y_t and vice versa, (C) Vector Auto-regression Model: X_t can cause Y_t and their lags, and vice versa, (D) Granger Causality Model-1: Y_t may be affected by changes in lag values at X_{t-1}, X_{t-2} and $X_{t-i...}$, and changes in lag values in Y_{t-1}, Y_{t-2} *and* Y_{t-j},.. where i and j represent different time points (E) Granger Causality Model-2: X_t may be affected by changes in lag values at Xt_{-1}, X_{t-2}, X_{t-i}... and changes in lag values in Y_{t-1}, Y_{t-2}, Y_{t-i}...

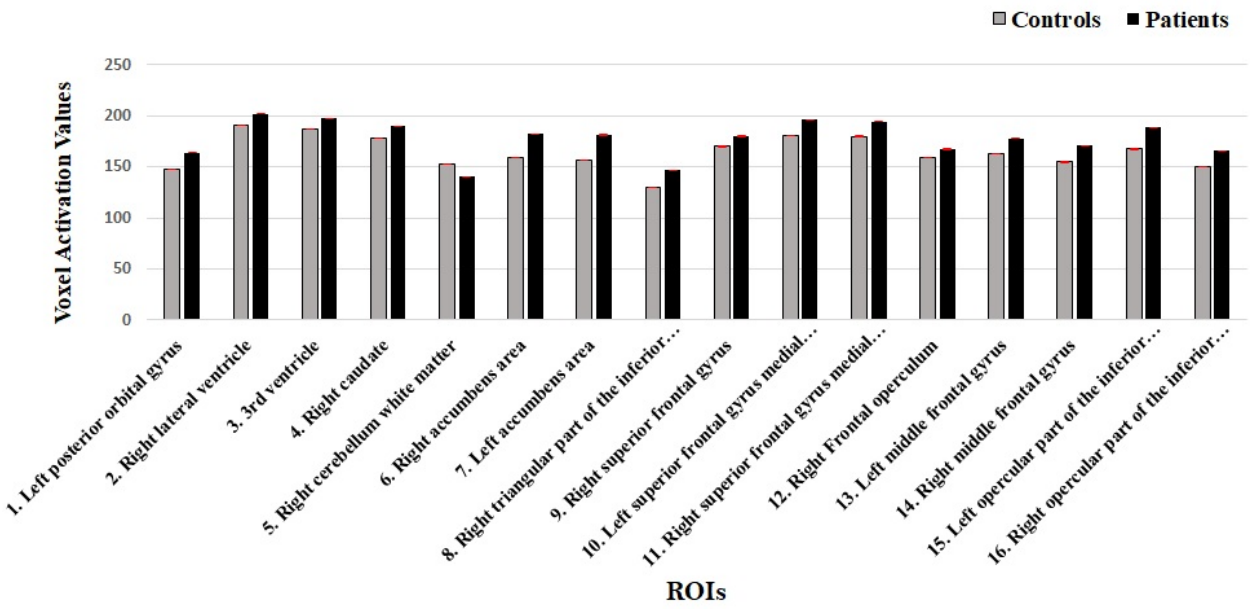

Figure 2 - Average Voxel Activation in Controls and Schizophrenia Patients. The bar graph shows average voxel activations in 16 ROIs for controls (grey) and patients (black).

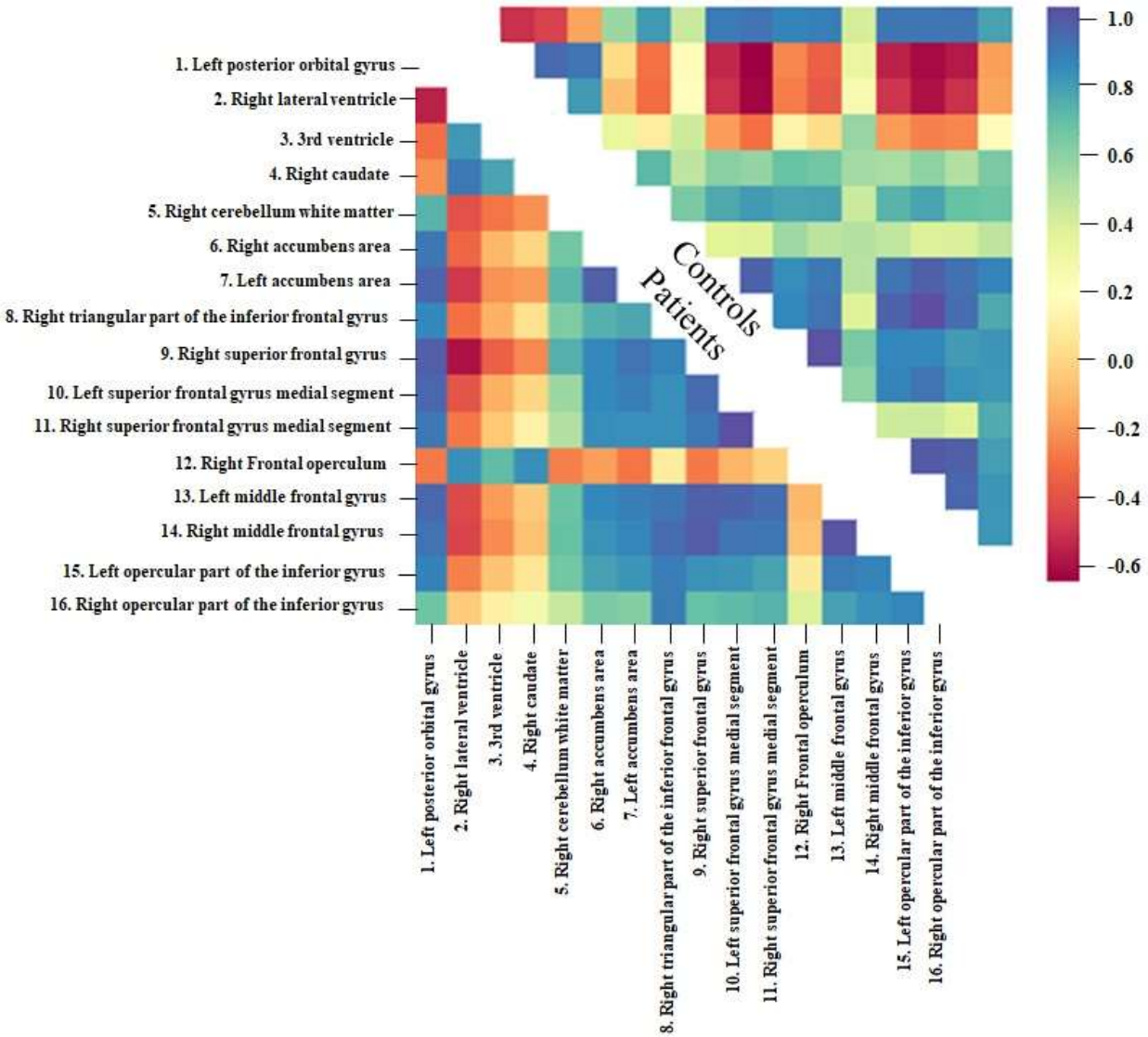

Figure 3 - Correlation Between ROIs in Controls and Schizophrenia Patients. The heat map shows Person correlation between the ROIs in controls and SZ patients.

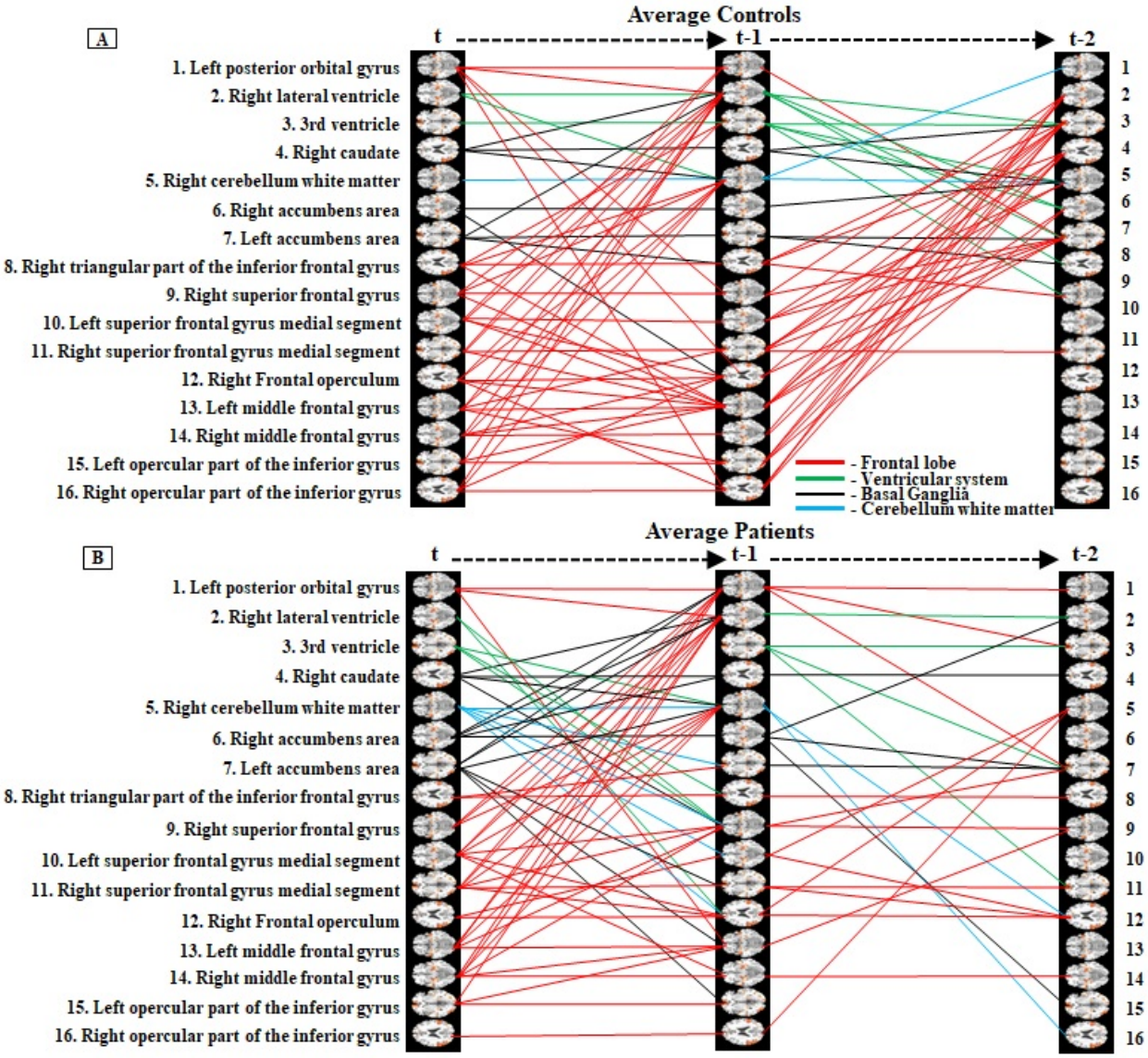

Figure 4 - Structural Connectivity in ROIs through vector autoregression model. Significant causality links between the ROIs in the patients (A) and the controls (B).

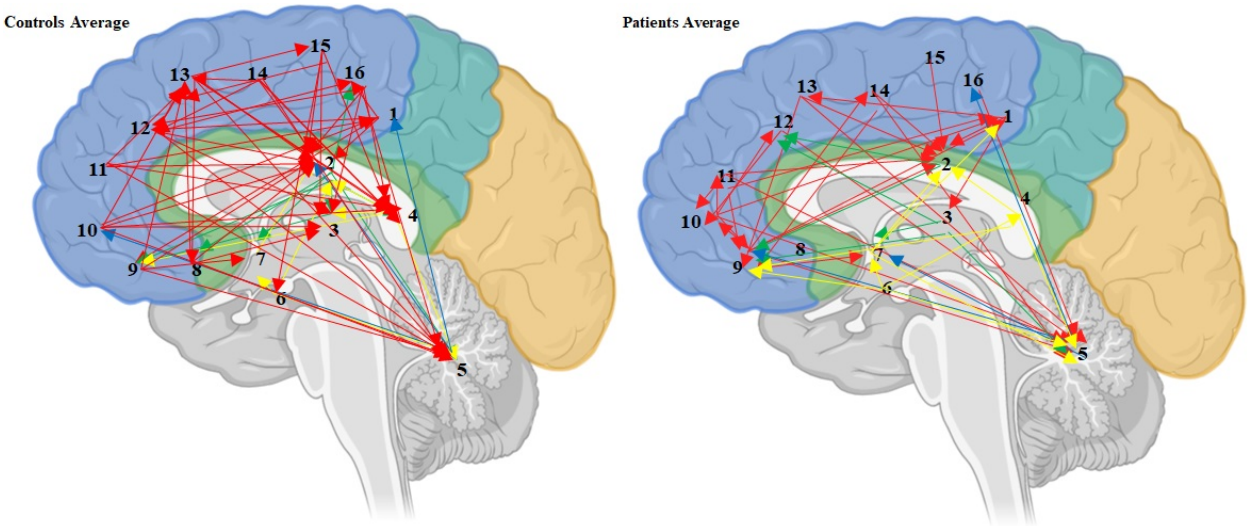

Figure 5 - Structural Connectivity in ROIs obtained through Granger Causality. Arrows show significant granger causality between ROIs for the controls (A) and patients (B).

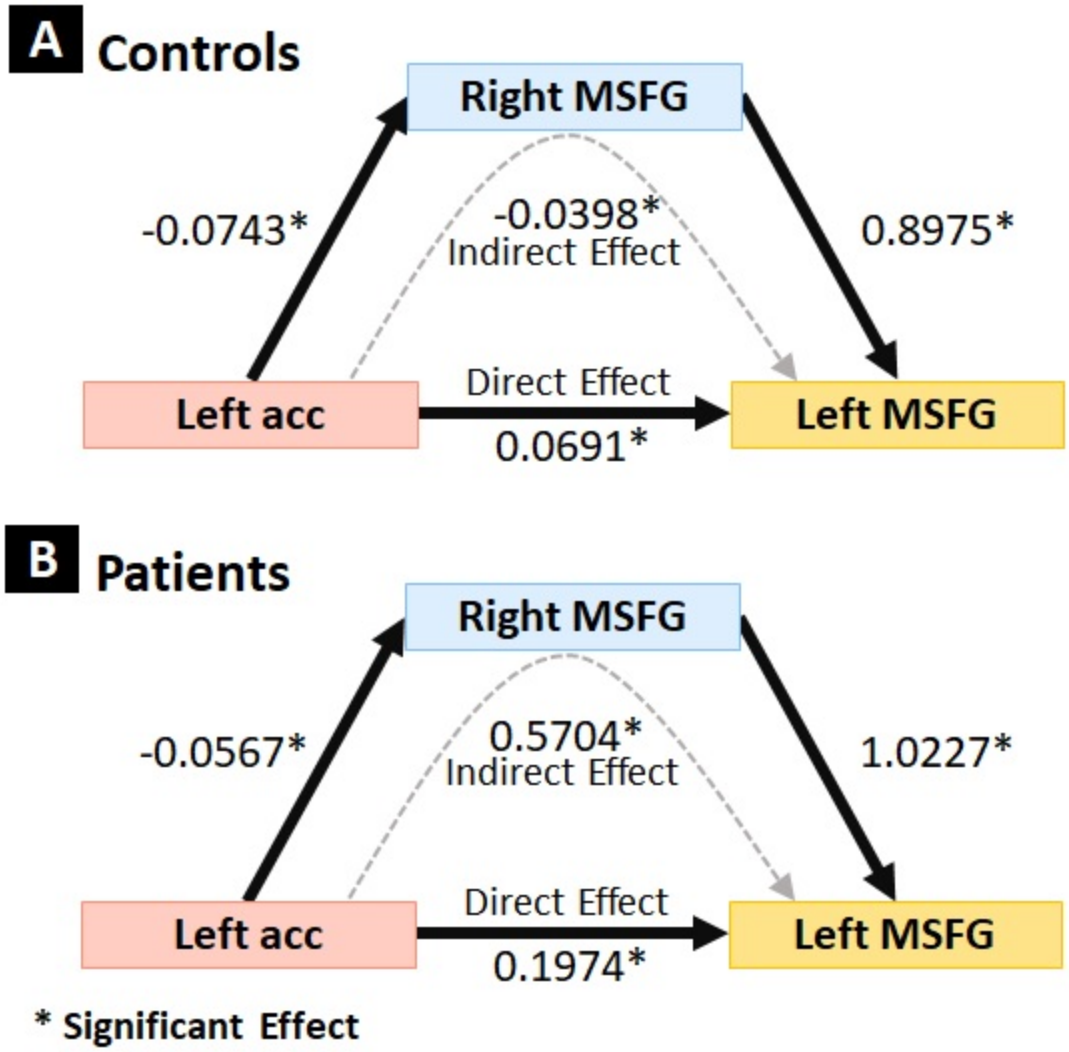

Figure 6 - Mediation Analysis. **(A)** Mediation in controls between Left accumbens area, right MSFG, and left MSFG, **(B)** Mediation in patients between Left accumbens area, right MSFG, and left MSFG.